Sinclair PB, Blair HH, Ryan SL, Buechler L, Cheng J, Clayton J, Hanna R, Hollern S, Hawking Z, Bashton M, Schwab CJ, Jones L, Russell LJ, Marr H, Carey P, Halsey C, Heidenreich O, Moorman AV, Harrison CJ.

Dynamic clonal progression in xenografts of acute lymphoblastic leukemia with intrachromosomal amplification of chromosome 21.

***Haematologica* 2018,**

https://doi.org/10.3324/haematol.2017.172304

Published Ahead of Print on February 15, 2018, as doi:10.3324/haematol.2017.172304.

EUROPEAN HEMATOLOGY ASSOCIATION

haematologica

Journal of the European Hematology Association
Owned & published by the Ferrata Storti Foundation

Dynamic clonal progression in xenografts of acute lymphoblastic leukemia with intrachromosomal amplification of chromosome 21

by Paul B. Sinclair, Helen H. Blair, Sarra L. Ryan, Lars Buechler, Joanna Cheng, Jake Clayton, Rebecca Hanna, Shaun Hollern, Zoe Hawking, Matthew Bashton, Claire J. Schwab, Lisa Jones, Lisa J. Russell, Helen Marr, Peter Carey, Christina Halsey, Olaf Heidenreich, Anthony V. Moorman, and Christine J. Harrison

Haematologica 2018 [Epub ahead of print]

Citation: Paul B. Sinclair, Helen H. Blair, Sarra L. Ryan, Lars Buechler, Joanna Cheng, Jake Clayton, Rebecca Hanna, Shaun Hollern, Zoe Hawking, Matthew Bashton, Claire J. Schwab, Lisa Jones, Lisa J. Russell, Helen Marr, Peter Carey, Christina Halsey, Olaf Heidenreich, Anthony V. Moorman, and Christine J. Harrison. Dynamic clonal progression in xenografts of acute lymphoblastic leukemia with intrachromosomal amplification of chromosome 21. Haematologica. 2018; 103: xxxdoi:10.3324/haematol.2017.172304

Dynamic clonal progression in xenografts of acute lymphoblastic leukemia with intrachromosomal amplification of chromosome 21.

Paul. B. Sinclair[1], Helen H. Blair[1], Sarra L. Ryan[1], Lars Buechler[1], Joanna Cheng[1], Jake Clayton[1], Rebecca Hanna[1], Shaun Hollern[1], Zoe Hawking[1], Matthew Bashton[1], Claire J. Schwab[1], Lisa Jones[1], Lisa J. Russell[1], Helen Marr[1], Peter Carey[2], Christina Halsey[3], Olaf Heidenreich[1], Anthony V. Moorman[1] and Christine J. Harrison[1].

[1]Wolfson Childhood Cancer Research Centre, Northern Institute for Cancer Research, Newcastle University, Newcastle-upon-Tyne, UK; [2]Department of Clinical Haematology, Royal Victoria Infirmary, Newcastle-upon-Tyne, UK; [3]Wolfson Wohl Cancer Research Centre, Institute of Cancer Sciences, University of Glasgow, Glasgow, UK.

Contact information for correspondence: Professor Christine Harrison PhD. FRCPath. FMedSci. Wolfson Childhood Cancer Research Centre, Northern Institute for Cancer Research, Level 6, Herschel Building, Brewery Lane, Newcastle-upon-Tyne NE1 7RU, UK. **Phone**: +44(0)191 208 2237 **FAX:** +44 (0)191 208 2246 **email**: christine.harrison@newcastle.ac.uk

Running head; iAMP21 Xenografts.

Abstract word Count; **247**

Main text word count; 3997

Acknowledgements.

The authors would like to thank the department of Cellular Medicine, Royal Victoria Infirmary, Newcastle-upon-Tyne NHS Foundation Trust for fixing and staining histological samples. Tracey Davey and Kath White, Electron Microscopy Research Services, Newcastle University for EM preparations and images and Clare Orange and Lynn Stevenson, University of Glasgow, for the brain

histology and imaging. The brain histology slides were scanned by Glasgow University slide scanning and image analysis service at the QEUH. We would also like to thank the Bloodwise Childhood Leukaemia Cell Bank for providing primary childhood leukaemia samples.

Abstract

Intrachromosomal amplification of chromosome 21 is a heterogeneous chromosomal rearrangement occurring in 2% of childhood precursor B-cell acute lymphoblastic leukemia. There are no cell lines with iAMP21 and these abnormalities are too complex to faithfully engineer in animal models. As a resource for future functional and pre-clinical studies, we have created xenografts from intrachromosomal amplification of chromosome 21 leukemia patient blasts and characterised them by *in-vivo* and *ex-vivo* luminescent imaging, FLOW immunophenotyping, and histological and ultrastructural analysis of bone marrow and the central nervous system. Investigation of up to three generations of xenografts revealed phenotypic evolution, branching genomic architecture and, compared with other B-cell acute lymphoblastic leukemia genetic subtypes, greater clonal diversity of leukemia initiating cells. In support of intrachromosomal amplification of chromosome 21 as a primary genetic abnormality, it was always retained through generations of xenografts, although we also observed the first example of structural evolution of this rearrangement. Clonal segregation in xenografts revealed convergent evolution of different secondary genomic abnormalities implicating several known tumour suppressor genes and a region, containing the B-cell adaptor, *PIK3AP1,* and nuclear receptor co-repressor, *LCOR*, in the progression of B-ALL. Tracking of mutations in patients and derived xenografts provided evidence for co-operation between abnormalities activating the RAS pathway in B-ALL and for their aggressive clonal expansion in the xeno-environment. Bi-allelic loss of the *CDKN2A/B* locus was recurrently maintained or emergent in xenografts and also strongly selected as RNA sequencing demonstrated a complete absence of reads for genes associated with the deletions.

Introduction.

Xenograft models of leukemia have been used to address a number of important fundamental and translational research questions relating to: the nature of leukemia stem cells, clonal evolution and experimental therapies.(1-8) Limiting dilution studies have demonstrated that leukemia initiating cells (LIC) are common, while fluorescence *in situ* hybridisation (FISH), genomic arrays, analysis of Ig/TCR rearrangements, immunophenotype and drug response have suggested that the disease can be propagated through multiple generations of mice with high fidelity.

Intrachromosomal amplification of chromosome 21 (iAMP21) is an intriguing cytogenetic abnormality, defining a specific subgroup of approximately 2% of childhood precursor B-cell acute lymphoblastic leukemia (B-ALL). Chromosome 21 genomic profiles, although highly variable, always involve amplifications, flanked by regions of normal copy number or deletion(9, 10). We have shown that the oncogenic potential of chromosome 21 is optimised through a combination of catastrophic sequence reorganisation, driven by chromothripsis, deletion and amplification, resulting from dicentric chromosome formation, breakage-fusion-bridge (BFB) cycles and whole chromosome arm duplications.(11) This mechanism has the potential to produce a near infinite number of alternative derivative chromosomes 21. The structure of the iAMP21 chromosome is stabilised by telomere acquisition or duplication, while a combination of protected amplified genes are postulated to confer an overall growth advantage, leading to the development of ALL. Several lines of evidence indicate that iAMP21 is a stable, primary genetic change: 1) among 530 patients, iAMP21 was reported as a sub-clonal abnormality in only a single case,(12) 2) the iAMP21 chromosome morphology remains consistent between cells in the same patient, 3) the same chromosome structure is observed at diagnosis and relapse.(9) A range of specific secondary genetic abnormalities: *CRLF2* activating rearrangements, X chromosome gain, deletions of *RB1*, *ETV6*, the long arm of chromosome 7 (7q) and 11q, and mutations of the *RAS* pathway frequently co-occur with iAMP21.(9, 12, 13)

This distinct iAMP21-ALL subgroup is clinically defined by older age (median 9 years), low white blood cell counts (WBC) and a high risk of relapse on standard therap.(14-16) Intensive therapy significantly reduced the relapse risk(17, 18) but associated morbidity highlights an urgent need for less toxic regimens. Development of rational targeted therapies requires understanding of the mechanism by which these rearrangements initiate leukemia. However the requisite tools for functional studies are lacking because no iAMP21-ALL cell lines exist and the complex nature of the abnormalities exclude their reproduction in engineered animal models. To address this shortfall, we transplanted primary leukemia cells from five iAMP21-ALL patients into NOD/LtSz-scid IL2Rγ null (NSG) mice. *In-vivo* luminescent imaging, to track the physical development of ALL, was used to assess these xenografts as potential models for functional and pre-clinical studies. In addition, we have characterised the disease morphology at the microscopic and ultrastructural level and, as a first application, have performed extensive genomic analysis to investigate clonal heterogeneity of iAMP21-ALL, from which some intriguing findings have emerged.

Methods.

Patients.

Viable cells from children diagnosed with iAMP21-ALL, as previously defined,(19) were provided by the Bloodwise Childhood Leukemia Cell Bank. Ethical approval was obtained for all patients and informed consent was granted in accordance with the Declaration of Helsinki. Karyotypes and demographic details of patients used to generate xenografts or as controls for histological analysis are presented in Supplementary Tables 1 - 3.

Xenografts and isolation of leukemia cells.

Primografts were created by intrafemoral injection of patient cells into NSG mice, as previously described.(1) Between $2x10^4$ and $2x10^6$ primograft bone marrow or spleen cells from each mouse were used in the same procedure to create 2° and 3° xenografts (Supplementary Table 4).

Xenografts were culled at end stage disease as defined in the online supplementary methods. Bone marrow cells flushed from femurs and disaggregated spleens were passed through 40µm cell strainers. Leukaemic cells used for all experimental work were purified from spleen preparations by separation over Ficol-Paque [density 1.077] (G.E. Health Care, Buckinghamshire, UK). Proportions of human and mouse cells and immunophenotypes of the human leukemia fractions were determined by flow cytometry as described in the online supplementary methods.

Lentiviral transduction, *in-vitro* culture and *in-vitro*, *in-vivo* and *ex-vivo* imaging of xenograft cells. Detailed procedures are provided in the online supplementary methods.

Histopathology and Transmission Electron Microscopy (TEM).

Detailed procedures are provided in the online supplementary methods.

SNP6.0 arrays.

DNA extraction and SNP6.0 array hybridisation and analysis was performed, as previously described.(13) To define regions of chromosome 21 copy number (CN) evolution, SNP CN values were subtracted between 2° xenografts F7897RN and F7897LN. CN abnormalities (CNA) in immunoglobulin or T-cell receptor regions, those not involving coding gene regions, present in patient remission sample or reported in the Toronto Database of Genomic Variants, were not reported. Genomic positions are for Hg19.

Fluorescence in situ hybridisation (FISH) and Multiplex Ligation-dependent Probe Amplification (MLPA).

Dual colour FISH on 100-200 interphase cells was performed using fluorescently labelled BAC probes hybridising to the *RUNX1* (RP11-773I18) and *APP* (RP11-66H5 and RP11-15D13) genomic regions or commercially available probes to the CDKN2A/B genomic region and chromosome 9 centromere

(CytoCell, Cambridge UK), as previously described.(20) MLPA was performed using the SALSA MLPA 335 kit (MRC-Holland, The Netherlands), as previously described.(21)

Analysis of RAS pathway mutations and RNA sequencing.

Detailed procedures are provided in the online supplementary methods.

Results.

Development of iAMP21-ALL xenografts and characterisation by *in-vivo* and *ex-vivo* imaging.

Of six primary and two relapsed cases of iAMP21-ALL transplanted into femurs of NSG mice, five, including one relapse case, developed ALL derived from the human cells, in one or more animals (Supplementary Table 1). Mean time to development of end stage disease in primografts was 30 weeks and splenomegaly was seen in all engrafted animals. 2° and 3° xenografts were established in three and one cases respectively, and all were assigned unique identifiers indicating passage number and patient of origin, for example 2°3e was one of several secondary xenografts derived from patient 3. Xenograft leukemia cells constituted between 40-92% of bone marrow and 23-53% and 79-99% of crude and purified spleen samples respectively (Supplementary Table 4). Essentially all human cells isolated from xenografts expressed the B-cell markers CD19 and CD10 but analysis of CD34 and CD38 demonstrated considerable phenotypic divergence between mice (supplementary table 5 and supplementary figure 1).

To investigate their potential for use in *in-vivo* and *in-vitro* functional studies, we transduced xenograft stocks from four iAMP21-ALL patients with the pSLIEW lentivirus vector that expresses luciferase and EGFP.(22) Three days after transduction, a total of $3x10^6$ cells from each patient were transplanted by intra-femoral injection into two NSG mice each, here identified by patient number followed by a^{SLIEW} or b^{SLIEW}. Less than 1% of transduced cells were GFP positive by FACS analysis at this time point (supplementary Figure 2) or by fluorescence microscopy after one week culture on MS-5 feeder layers (data not shown), nevertheless, by 2-4 weeks following transplant, luminescent

signals, clearly localised to the injected femurs, were seen on whole body imaging of all mice. Leukemia spread to other bones and organs with noticeable variation in the strength of signal at some sites (Supplementary Figure 3). This variation was highlighted by measurement of luminescent signals from organs post mortem and by analysis of the relationship between signal development at different sites over time (Figures 1A, 1B and table 1). In spleen signal variation was shown to relate to the proportion of infiltrating blast cells that expressed EGFP rather than to overall tumour load (Figures 1C, Table 1 and Supplementary Table 4). Serial 3D reconstruction of one xenograft showed dramatic increases in signals from the spleen and head between weeks 11-15 (Figure 1D).

Morphology and ultrastructure of bone marrow and CNS reveals patient specific heterogeneity, including evidence for systemic bone marrow niche destruction.

To investigate bone marrow morphology and CNS involvement in the iAMP21-ALL models, we examined sections through tibias, sternums and heads of the mice engrafted with SLIEW transduced cells. H&E stained control NSG bone marrow resembled that of a wild type mouse(23) and was negative for anti-human CD19, CD45 and Ki-67 staining (Figure 2A and Supplementary Figure 4). In xenografts, two types of morphology were seen, both of which differed from controls; type A, which closely resembled that of iAMP21-ALL patient trephines (Figures 2B, 2G, Supplementary Figures 4 and 5 and Supplementary table 2) and type B, which although abnormal, clearly differed from the patient trephines (Figures 2C, 2G and Supplementary Figure 4). Cells in type A but not type B sections were actively cycling and of human origin as indicated by staining with anti-human Ki67, CD19 and CD45 antibodies (Figures 2D and Supplementary Figure 4). Individual sections presented with either type A or B morphology only with the exception of one sternum segment where both types co-existed (Figure 2D). There was relatively sharp demarcation between the A and B type areas, suggesting that the iAMP21 ALL cells were organized into massive clumps that didn't easily diffuse within the lumen.

From different tibia or forelimb bones of each mouse, we performed TEM of decalcified sections. Xenograft ultrastructure always differed from wild type controls and, as with bright field microscopy, two distinct categories could be identified (Figure 2E and Supplementary Figure 6). The first was termed viable leukemia (VL), as mitotic figures were present and cells appeared normal, although homogeneous by comparison with controls. There were more connections and less extracellular space between cells in preparations from 4a/b^{SLIEW} compared with controls and 1a/b^{SLIEW}. The second category, equivalent to histological type B, was termed apoptotic (AP), as no mitotic figures were present and cells were depleted in number with classical signs of apoptosis, in the form of condensed chromatin localised to the periphery of the nucleus.(24)

We also examined sections through the skulls and CNS of seven of the eight xenografts (Figures 2F and Supplementary Figure 7), revealing calvaria in all cases, packed with homogeneously stained cells resembling the A type morphology of tibia sections. CNS involvement ranged from small foci of leukemia cells to heavy meningeal infiltration, extending into the choroid plexus in one case. Comparison of CNS histological grades for each xenograft with bone marrow histopathology and TEM data (Table 2) showed heavy CNS involvement only in 1a/b^{SLIEW} and 4a/b^{SLIEW}, correlating with fibia marrow histological type A and TEM type VL. We infer the proportion of transduced cells infiltrating the CNS varied between mice because luminescent signals from the head failed to correlate with histological grade (Table 2).

To investigate the relative incidence of the morphological types we examined H&E and anti CD19 stained bone marrow sections from 13 additional xenografts derived from seven B-ALL patients (Supplementary Tables 3 and 6). Among these cases, type B morphology was seen in two primografts, one derived from a relapsed iAMP21-ALL patient and the second from a case with high hyperdiploid ALL, areas of A type morphology were also seen in both (Supplementary Figure 8). Other xenografts displayed A type morphology either exclusively (Supplementary Figure 9) or infiltrating apparently normal mouse bone marrow (Supplementary Figure 10). Interestingly these

latter cases supported our initial observation that the ALL cells may grow in clumps because CD19+ve cells formed distinct clusters.

Segregation of CNA in xenografts implicates known and novel genes in the progression of iAMP21-ALL.

We used SNP6.0 array profiles to evaluate the genomic stability of iAMP21-ALL in 21 xenografts from five patients. Presentation and remission samples were available for all except patient 4. A core of 3-16 concordant CNA, involving coding gene regions, were clonal at presentation and retained in all xenografts (Supplementary Table 7). The existence of competing sub-clones and branching genomic evolution was demonstrated by discordant CNA, which occurred at a rate of between 4 and 12 (Figure 3 and Supplementary Table 7). Clonal trisomies or copy number neutral loss of heterozygosity (CN-LOH), present in each patient sample, were lost after transplant, while deletions and amplifications were typically sub-clonal and either lost or increased in level or newly emergent as sub-clones in xenografts. Exceptionally in xenografts of patient 1, a sharp transition in genomic architecture, involving clonal gain of CNA of three chromosomes, occurred. Chromosome 21 profiles usually remained unchanged across samples (Supplementary Figure 11), but interestingly in cells from patient 1, we observed structural evolution of the iAMP21 chromosome, involving a small region of copy number gain and nine distinct regions of loss of one or two copies (Figure 3A and Supplementary Table 8). Importantly the additional deletions did not affect two regions predicted to contain critical oncogenes(11) but did re-define the proximal boundary of the region of highest level of amplification(9) from 21:32,813,553-37 to 21:33,949,423. By FISH, we confirmed that the *RUNX1* and *APP* gene regions were maintained at the same level of amplification and reduced in copy number from three to one, respectively. Additional rearrangements included bi-allelic deletion of the short arm of chromosome 9 (9p), resulting in homozygous loss of *CDKN2A/B,* as confirmed by MLPA (Supplementary Table 9), and mono-allelic deletion of 3p, involving the *CMTM* genes 6-8. SNP6.0 array and FISH provided no evidence of these CNA prior to their emergence in 2°1a.

However, as previously reported, two reads in whole genome sequencing data were consistent with the presence of a minor clone carrying the chromosome 3 deletion in the patient cells at presentation.(11)

Suggestive of convergent clonal evolution and highlighting the relevance of specific chromosomal regions to disease progression, several were targeted by different abnormalities segregated in xenografts from the same patient. Consistent with an oncogenic role for genes on Xp, patient 2 carried competing sub-clones marked by gain of a whole X chromosome or isochromosome Xp (Figure 3B). Whether emergence of a focal deletion of Xp, involving the zinc finger genes, *ZNF157* and *ZNF41,* was related to the presence of the larger scale CNA remains unclear but they were unlikely to have been driven by *CRLF2* overexpression, as genetic analysis ruled out rearrangement of this locus in the patient sample(25). In patient 3 large overlapping deletions of 12p, both involving *ETV6*, were segregated (Figure 3C). Although no patient material was available, revealing differences in CNAs involving the long arm of chromosome 10 were identified in xenografts from a relapse sample of patient 4 (Figure 3D). Strongly indicative for convergent evolution and hence a role in leukemia progression, the same focal bi-allelic deletion, involving *PIK3AP1* (*BCAP*) and *LCOR* (C10orf21), was nested within two distinctly different, large, mono-allelic 10q deletions. Evidently of independent origin, as it was detected only in a single xenograft, one of the large deletions also harboured a second likely co-operating focal bi-allelic deletion that resulted in loss of *BLNK*. Lastly passage of patient 5 cells in a primary xenograft resulted in concomitant loss of CN-LOH of 12q, with progression from sub-clonal to clonal deletion of a region of 12q containing *SH2B3* (Figure 3E). Comparison between relapse and the xenograft showed no overlap in progression of specific CNA, although interestingly the *EBF1* gene was targeted by different deletions in the two samples.

Mutations affecting the RAS pathway drive clonal expansion.

To investigate progression of mutations activating the RAS pathway previously identified in patient 1(13) we performed whole exome sequencing of selected and Sanger sequencing of all derived

xenografts (Fig 4a). Interestingly while an *NF1* mutation remained clonal in all samples, two different mutations affecting *NRAS* and one of *KRAS* marked a dramatic clonal evolution. Remarkably the KRAS mutation, present as a dominant clone in both primary and one secondary xenograft was undetectable at a read depth of over 6000 in the presentation sample and also undetected in other xenografts which instead carried a dominant *NRAS* mutation detected in only 1% of reads at presentation. *NRAS* and *FLIT3* mutations detected at presentation in patients 3 and 5 respectively were clonal in xenografts while the *FLIT3* mutation was lost at relapse (Figures 4b and 4c).

Transcriptional environment associated with deletions.

Anticipating that xenograft preparations, in contrast to patient samples, would be free of non-leukemic human cells, we used them to investigate the transcriptional environment associated with bi-allelic deletions (Table 3). By comparison with non-deleted samples, and confirming clonal dominance of the chromosome 10 deletions, we saw marked reductions in the levels of transcription of *PI3KAP1*, *LCOR* and *BLNK*. Loss of the *BLNK* genomic region also resulted in silencing of *DNTT* and *OPALIN*. Three of the four sequenced xenografts carried bi-allelic 9p deletions affecting *CDKN1A/B*. Indicating strong pressure for clonal selection of bi-allelic loss, read counts within this region were reduced to zero in deleted cases. Interestingly two focal bi-allelic deletions were associated with silencing not only of the physically deleted genes but also of *TUSC1,* positioned more than 3 Mb away from the deletion boundaries.

Discussion

Compared with genetically engineered animal models, xenografts bring several advantages to the study of ALL, not least, their potential to fully recapitulate the spectrum of genomic abnormalities that occur within individual patients of a given genetic sub-type. This is particularly relevant to iAMP21-ALL, where the primary abnormality is structurally complex, unique to each patient and impossible to reproduce in engineered animal models. As there are no cell lines carrying iAMP21,

the xenografts presented here represent an important resource for future functional and pre-clinical studies.

Highlighting the potential of lentiviral constructs integrated into xenograft cells, we demonstrated their *in vivo* expression. However we observed considerable temporal and spatial variation in signal development that, as demonstrated by analysis of spleen and CNS, was apparently related to heavy skewing of the ratios of transduced to non-transduced cells at specific sites. It seems likely that this skewing was caused largely by clonal expansion of small founder populations, particularly as tracking of specific genomic abnormalities demonstrated aggressive expansion of minor sub-clones in xenografts. As a consequence, accurate analysis of disease burden by in-vivo imaging, will in future require enrichment for *EGFP* expressing cells prior to engraftment.

Unexpectedly, light microscopy and TEM together provided strong evidence that transplantation of NSG mice with iAMP21-ALL cells from two patients led to destruction of the bone marrow niche. As we saw no examples of similar morphology among iAMP21-ALL patient samples, it seemed likely that this phenomenon was xenograft specific and a consequence of initiating a heavy leukemic burden at one site. Cells populating the affected areas, although damaged, were heterogeneous and showed little if any staining with human CD19 and CD45 suggesting they were of host origin. Histology was therefore consistent with destruction having occurred in areas of normal bone marrow before malignant cell infiltration suggesting systemic suppression of normal haematopoiesis, possibly through a mechanism such as cytokine scavenging, as recently reported to account for cytopenia in AML.(26) The effect did not correlate with late stage disease, as mean time between transplant and cull were almost identical and spleen weights were higher and CNS infiltration heavier for mice with no evidence of niche destruction. Further analysis demonstrated that niche destruction is not restricted to the iAMP21-ALL sub-type but is probably less common than suggested by our initial data.

Global analysis of iAMP21-ALL patient and xenograft genomes revealed a dynamic branching of genomic architecture, similar to that reported previously for B-ALL.(4, 6, 7, 27, 28) However the rate of newly emergent CNA and their diversity in iAMP21-ALL xenografts suggested a LIC compartment characterised by greater genetic heterogeneity compared with other B-ALL sub-types. Genomic arrays revealed an average of five CNA changes per transplanted iAMP21-ALL sample, while similar analysis defined only a single change among seven *KMT2A* rearranged infant ALL samples engrafted into multiple mice.(28) Additionally, among 12 BCR-ABL1-positive ALL samples, half showed no CNA discordance in xenografts.(27) The iAMP21-ALL primografts also developed disease with a relatively long latency. Together with the older patient age at diagnosis of iAMP21-ALL(12), these data suggest that the primary iAMP21 rearrangement confers only a moderate growth advantage, producing an indolent disease course over which diverse genetic sub-clones are sampled. As genetic diversity has been linked to clinical aggressiveness,(29) this clonal heterogeneity of iAMP21-ALL may underlie their poor response to standard therapy.(17)

Although each iAMP21 chromosome is unique with respect to the balance of regions amplified and deleted, within clinical trials, these patients are treated homogeneously.(17) Our data support this approach, as they further confirm iAMP21 to be a primary abnormality, because the region identified as consistently amplified and spared from chromothripsis,(11) was always retained. However in xenografts from one patient, we observed segregation of a structurally evolved iAMP21 chromosome which, together with other CNA, marked a clone that appeared to confer an exceptionally strong growth advantage. Structural evolution of iAMP21 has not been reported previously, although only few presentation/relapse pairs have been analysed at the whole genome level and FISH is usually targeted only to the *RUNX1* gene. This case demonstrates that even after stabilisation of the iAMP21 chromosome evident at the time of diagnosis, these rearrangements can undergo further evolution, potentially influencing clinical features and treatment response. However this iAMP21 chromosome may be atypical, as it was reported to be a ring chromosome, which are known to be inherently unstable structures.(30) It may be that other iAMP21 ring chromosomes

have a tendency to further evolution, but this case was the only one included in this study. Whether this iAMP21 chromosomal evolution acted as a driver of leukemia progression remains uncertain, as it was co-selected with other abnormalities, including an NRAS mutation and bi-allelic loss of *CDKN2A/B*. Among the four other cases transplanted, three were affected by concordant or discordant *CDKN2A* deletions, two bi-allelic and one mono-allelic, detected by MLPA only and without apparent involvement of *CDKN2B*. Further suggesting strong selective pressure for loss of *CDKN2A/B* in the xenografts, as evidenced by RNA sequencing data, the bi-allelic deletions were all highly clonal. As deletion of this locus only occurs in about 12% of iAMP21-ALL patients(21), these observations support previous reports that *CDKN2A/B* loss is associated with rapid disease manifestation(27) and is selected for in B-ALL xenografts,(4) and are also in keeping with a xenograft specific expression signature enriched for cell cycle genes.(31) Alternative mutations of *NRAS* and *KRAS* were also strongly selected and both apparently co-operated with an NF1 mutation in xenografts. To our knowledge NF1 and RAS mutations have always been reported as mutually exclusive in B-ALL patients, although their co-occurrence in Juvenile myelomoncytic leukemia has been associated with aggressive disease. In mouse models, a combination of *NF1* deficiency and *KRAS* activating mutation reduced the latency of myeloid malignancy compared with either abnormality alone (13, 32, 33).

Other chromosomal regions were strongly implicated in ALL progression, as targets of overlapping abnormalities segregated in different clones of xenografts. These included genes known to be involved in B-ALL; *ETV6*, *SH2B3* and *BLNK (SLP-65),*(34-36) as well as novel candidate tumour suppressor genes. Two distinct large deletions, selected in different xenografts, resulted in conversion to homozygosity of a micro-deletion involving *PIK3AP1* and *LCOR*. *PIK3AP1* encodes an adaptor protein linking the B-cell receptor (BCR) and CD19 to activation of PI3K/Akt.(37-39) A similar function in the transduction of pre-BCR signalling is likely and, although not previously implicated in childhood leukemia, focal deletions of *PIK3AP1* have been reported in three cases of adult B-ALL.(40, 41) Combined with our evidence for strong selective pressure for its conversion from mono to bi-

allelic deletion, *PIK3AP1* is an interesting candidate, possibly worthy of addition to the growing list of pre-BCR related genes disrupted in childhood B-ALL.(42) However a role for *LCOR,* which functions as a co-repressor of several nuclear hormone receptors,(43) and has been reported to interact with methyltransferase complexes including polycomb repressive complex 2,(44) should not be discounted.

In conclusion, we present the first successful xenografts of iAMP21-ALL and demonstrate their potential as experimental models for functional investigation of this poorly understood genetic subtype. These xenografts could also serve as models in pre-clinical trials or for personalised medicine, with the caveat that systemic niche destruction occurred in some cases. Tracking of CN abnormalities, to investigate genomic evolution in xenografts, revealed a surprisingly high rate of instability and examples of marked divergence in CN status of known leukemia driver genes. Further genomic screening of iAMP21-ALL xenografts is likely to reveal many more clonal abnormalities undetected in patient samples, augmenting data generated from clinical trial cohorts, as well as potentially guiding treatment in individual cases.

References

1. Rehe K, Wilson K, Bomken S, et al. Acute B lymphoblastic leukaemia-propagating cells are present at high frequency in diverse lymphoblast populations. EMBO Mol Med. 2013;5(1):38-51.
2. Barrett DM, Seif AE, Carpenito C, et al. Noninvasive bioluminescent imaging of primary patient acute lymphoblastic leukemia: a strategy for preclinical modeling. Blood. 2011;118(15):e112-117.
3. Morisot S, Wayne AS, Bohana-Kashtan O, et al. High frequencies of leukemia stem cells in poor-outcome childhood precursor-B acute lymphoblastic leukemias. Leukemia. 2010;24(11):1859-1866.
4. Schmitz M, Breithaupt P, Scheidegger N, et al. Xenografts of highly resistant leukemia recapitulate the clonal composition of the leukemogenic compartment. Blood. 2011;118(7):1854-1864.
5. Terziyska N, Castro Alves C, Groiss V, et al. In vivo imaging enables high resolution preclinical trials on patients' leukemia cells growing in mice. PLoS One. 2012;7(12):e52798.
6. Anderson K, Lutz C, van Delft FW, et al. Genetic variegation of clonal architecture and propagating cells in leukaemia. Nature. 2011;469(7330):356-361.

7. Patel B, Dey A, Castleton AZ, et al. Mouse xenograft modeling of human adult acute lymphoblastic leukemia provides mechanistic insights into adult LIC biology. Blood. 2014;124(1):96-105.
8. Townsend EC, Murakami MA, Christodoulou A, et al. The Public Repository of Xenografts Enables Discovery and Randomized Phase II-like Trials in Mice. Cancer Cell. 2016;29(4):574-586.
9. Rand V, Parker H, Russell LJ, et al. Genomic characterization implicates iAMP21 as a likely primary genetic event in childhood B-cell precursor acute lymphoblastic leukemia. Blood. 2011;117(25):6848-6855.
10. Strefford JC, van Delft FW, Robinson HM, et al. Complex genomic alterations and gene expression in acute lymphoblastic leukemia with intrachromosomal amplification of chromosome 21. Proc Natl Acad Sci U S A. 2006;103(21):8167-8172.
11. Li Y, Schwab C, Ryan SL, et al. Constitutional and somatic rearrangement of chromosome 21 in acute lymphoblastic leukaemia. Nature. 2014;508(7494):98-102.
12. Harrison CJ, Moorman AV, Schwab C, et al. An international study of intrachromosomal amplification of chromosome 21 (iAMP21): cytogenetic characterization and outcome. Leukemia. 2014;28(5):1015-1021.
13. Ryan SL, Matheson E, Grossmann V, et al. The role of the RAS pathway in iAMP21-ALL. Leukemia. 2016;30(9):1824-1831.
14. Robinson HM, Broadfield ZJ, Cheung KL, et al. Amplification of AML1 in acute lymphoblastic leukemia is associated with a poor outcome. Leukemia. 2003;17(11):2249-2250.
15. Moorman AV, Richards SM, Robinson HM, et al. Prognosis of children with acute lymphoblastic leukemia (ALL) and intrachromosomal amplification of chromosome 21 (iAMP21). Blood. 2007;109(6):2327-2330.
16. Attarbaschi A, Mann G, Panzer-Grumayer R, et al. Minimal residual disease values discriminate between low and high relapse risk in children with B-cell precursor acute lymphoblastic leukemia and an intrachromosomal amplification of chromosome 21: the Austrian and German acute lymphoblastic leukemia Berlin-Frankfurt-Munster (ALL-BFM) trials. J Clin Oncol. 2008;26(18):3046-3050.
17. Moorman AV, Robinson H, Schwab C, et al. Risk-directed treatment intensification significantly reduces the risk of relapse among children and adolescents with acute lymphoblastic leukemia and intrachromosomal amplification of chromosome 21: a comparison of the MRC ALL97/99 and UKALL2003 trials. J Clin Oncol. 2013;31(27):3389-3396.
18. Heerema NA, Carroll AJ, Devidas M, et al. Intrachromosomal amplification of chromosome 21 is associated with inferior outcomes in children with acute lymphoblastic leukemia treated in contemporary standard-risk children's oncology group studies: a report from the children's oncology group. J Clin Oncol. 2013;31(27):3397-3402.
19. Harrison CJ, Haas O, Harbott J, et al. Detection of prognostically relevant genetic abnormalities in childhood B-cell precursor acute lymphoblastic leukaemia: recommendations from the Biology and Diagnosis Committee of the International Berlin-Frankfurt-Munster study group. Br J Haematol. 2010;151(2):132-142.
20. Schwab C, Harrison CJ. Acute lymphoblastic leukaemia. Methods Mol Biol. 2011;730:99-117.
21. Schwab CJ, Chilton L, Morrison H, et al. Genes commonly deleted in childhood B-cell precursor acute lymphoblastic leukemia: association with cytogenetics and clinical features. Haematologica. 2013;98(7):1081-1088.
22. Bomken S, Buechler L, Rehe K, et al. Lentiviral marking of patient-derived acute lymphoblastic leukaemic cells allows in vivo tracking of disease progression. Leukemia. 2013;27(3):718-721.
23. Travlos GS. Normal structure, function, and histology of the bone marrow. Toxicol Pathol. 2006;34(5):548-565.
24. Elmore S. Apoptosis: a review of programmed cell death. Toxicol Pathol. 2007;35(4):495-516.

25. Russell LJ, Capasso M, Vater I, et al. Deregulated expression of cytokine receptor gene, CRLF2, is involved in lymphoid transformation in B-cell precursor acute lymphoblastic leukemia. Blood. 2009;114(13):2688-2698.
26. Rauch PJ, Ellegast JM, Widmer CC, et al. MPL expression on AML blasts predicts peripheral blood neutropenia and thrombocytopenia. Blood. 2016;128(18):2253-2257.
27. Notta F, Mullighan CG, Wang JC, et al. Evolution of human BCR-ABL1 lymphoblastic leukaemia-initiating cells. Nature. 2011;469(7330):362-367.
28. Bardini M, Woll PS, Corral L, et al. Clonal variegation and dynamic competition of leukemia-initiating cells in infant acute lymphoblastic leukemia with MLL rearrangement. Leukemia. 2015;29(1):38-50.
29. Park SY, Gonen M, Kim HJ, Michor F, Polyak K. Cellular and genetic diversity in the progression of in situ human breast carcinomas to an invasive phenotype. J Clin Invest. 2010;120(2):636-644.
30. Guilherme RS, Meloni VF, Kim CA, et al. Mechanisms of ring chromosome formation, ring instability and clinical consequences. BMC Med Genet. 2011;12:171.
31. Clappier E, Gerby B, Sigaux F, et al. Clonal selection in xenografted human T cell acute lymphoblastic leukemia recapitulates gain of malignancy at relapse. J Exp Med. 2011;208(4):653-661.
32. Caye A, Strullu M, Guidez F, et al. Juvenile myelomonocytic leukemia displays mutations in components of the RAS pathway and the PRC2 network. Nat Genet. 2015;47(11):1334-1340.
33. Cutts BA, Sjogren AK, Andersson KM, et al. Nf1 deficiency cooperates with oncogenic K-RAS to induce acute myeloid leukemia in mice. Blood. 2009;114(17):3629-3632.
34. Moriyama T, Metzger ML, Wu G, et al. Germline genetic variation in ETV6 and risk of childhood acute lymphoblastic leukaemia: a systematic genetic study. Lancet Oncol. 2015;16(16):1659-1666.
35. Perez-Garcia A, Ambesi-Impiombato A, Hadler M, et al. Genetic loss of SH2B3 in acute lymphoblastic leukemia. Blood. 2013;122(14):2425-2432.
36. Jumaa H, Bossaller L, Portugal K, et al. Deficiency of the adaptor SLP-65 in pre-B-cell acute lymphoblastic leukaemia. Nature. 2003;423(6938):452-456.
37. Inabe K, Kurosaki T. Tyrosine phosphorylation of B-cell adaptor for phosphoinositide 3-kinase is required for Akt activation in response to CD19 engagement. Blood. 2002;99(2):584-589.
38. Okada T, Maeda A, Iwamatsu A, Gotoh K, Kurosaki T. BCAP: the tyrosine kinase substrate that connects B cell receptor to phosphoinositide 3-kinase activation. Immunity. 2000;13(6):817-827.
39. Castello A, Gaya M, Tucholski J, et al. Nck-mediated recruitment of BCAP to the BCR regulates the PI(3)K-Akt pathway in B cells. Nat Immunol. 2013;14(9):966-975.
40. Okamoto R, Ogawa S, Nowak D, et al. Genomic profiling of adult acute lymphoblastic leukemia by single nucleotide polymorphism oligonucleotide microarray and comparison to pediatric acute lymphoblastic leukemia. Haematologica. 2010;95(9):1481-1488.
41. Safavi S, Hansson M, Karlsson K, Biloglav A, Johansson B, Paulsson K. Novel gene targets detected by genomic profiling in a consecutive series of 126 adults with acute lymphoblastic leukemia. Haematologica. 2015;100(1):55-61.
42. Eswaran J, Sinclair P, Heidenreich O, et al. The pre-B-cell receptor checkpoint in acute lymphoblastic leukaemia. Leukemia. 2015;29(8):1623-1631.
43. Fernandes I, Bastien Y, Wai T, et al. Ligand-dependent nuclear receptor corepressor LCoR functions by histone deacetylase-dependent and -independent mechanisms. Mol Cell. 2003;11(1):139-150.
44. Alekseyenko AA, Gorchakov AA, Kharchenko PV, Kuroda MI. Reciprocal interactions of human C10orf12 and C17orf96 with PRC2 revealed by BioTAP-XL cross-linking and affinity purification. Proc Natl Acad Sci U S A. 2014;111(7):2488-2493.

Table 1. ***In-vivo*** **and** ***ex-vivo*** **luminescent imaging data and spleen weights for xenografts transplanted with iAMP21-ALL cells transduced with pSLIEW.**

Xenograft	Whole Body Luminescence (photons/second)			Dissected Organ Luminescence (photons/second)				Spleen weight/ % GFP +ve blasts*
	Peak whole body (PWB)	Peak injected femur (PIF)	Ratio PWB/PIF	Spleen	Liver	Kidney (mean)	Spleen radiance/g	
4^{SLIEW}a	6.87E+08	2.53E+08	2.72	ND	ND	ND	ND	0.83g / 0.2
4^{SLIEW}b	2.97E+08	5.09E+07	5.84	ND	ND	ND	ND	0.81g / 0.0
3^{SLIEW}a	1.64E+09	1.90E+08	8.63	5.69E+08	3.77E+07	1.49E+05	2.47E+09	0.23g / 44
3^{SLIEW}b	1.81E+09	4.00E+08	4.53	3.85E+08	1.99E+07	3.02E+05	1.43E+09	0.27g / 68%
1^{SLIEW}a	3.79E+08	2.44E+07	15.53	1.12E+07	4.10E+06	2.50E+05	2.11E+07	0.53g / 1.6%
1^{SLIEW}b	1.57E+08	1.43E+07	10.83	2.60E+07	4.27E+06	1.84E+05	2.95E+07	0.88g / 0.8%
2^{SLIEW}a	3.30E+09	1.06E+08	31.13	1.04E+09	9.84E+07	3.67E+05	2.60E+09	0.40g / 24%
2^{SLIEW}b	3.65E+09	3.64E+08	10.03	3.10E+09	1.83E+08	6.65E+05	5.64E+09	0.55g / 26%

*blasts are CD19 +ve cells isolated from spleen.

Table 2: Summary of histological and ultrastructural (EM) data for bone marrow and CNS of mice transplanted with iAMP21-ALL cells.

Xenograft	Tibia/sternum					Calvaria		CNS	
	H&E	CD19	CD45	Ki67	EM	H&E	CD19	(grade)	Peak head luminescence*
4a^{SLIEW}	A	+ve	+ve	+ve	VL	N/A	+ve	N/A	$8.3x10^7$
4b^{SLIEW}	A	+ve	+ve	+ve	VL	A	+ve	5	$3.4x10^7$
3a^{SLIEW}	A	+ve	-ve	+ve	AP	A	+ve	1-2	$3.4x10^8$
3b^{SLIEW}	A/B	+/-ve	-ve	+/-ve	AP	A	+ve	1-2	$2.3x10^8$
1a^{SLIEW}	A	+ve	+ve	+ve	VL	A	+ve	3-4 + CP	$3.7x10^7$
1b^{SLIEW}	A	+ve	+ve	+ve	VL	A	+ve	4	$6.4x10^6$
2a^{SLIEW}	A	+ve	-ve	+ve	AP	A	+ve	1	$3.7x10^8$
2b^{SLIEW}	B	-ve	-ve	-ve	AP	A	+ve	2	$6.3x10^8$

*Units of luminescence are total flux (photons / second).

Table 3. The expression of genes in xenograft derived iAMP21-ALL cells within and neighbouring regions of bi-allelic deletion of chromosomes 10 and 9.

Chromosome 10		Xenograft							
		3°1e		1°4b		2°2e		2°3d	
Gene	**Genomic position**	**RCM**	**CN**	**RCM**	**CN**	**RCM**	**CN**	**RCM**	**CN**
ZNF518A	*96,129,715-96,205,288*	3513	2	2746	1	2474	2	3316	2
BLNK	*96,191,702-96,271,587*	18573	2	21	0	11315	2	6251	2
DNTT	*96,304,396-96,338,564*	166450	2	344	1	170269	2	215495	2
OPALIN	*96,343,216-96,359,365*	458	2	2	1	698	2	471	2
TLL2	*96,364,606-96,513,918*	235	2	1	1	152	2	111	2
TM9SF3	*96,518,109-96,587,452*	14506	2	8325	1	12641	2	19522	2
PIK3AP1	*96,593,312-96,720,514*	35985	2	4	0	20616	2	28820	2
LCOR	*96,832,260-96,981,043*	8942	2	21	0	7568	2	4218	2
SLIT1	*96,998,038-97,185,920*	0	2	0	1	0	2	0	2
ARHGAP19	*97,222,173-97,292,673*	2486	2	4151	1	3164	2	3524	2
Chromosome 9									
MTAP	*21,802,543-21,937,651*	1	0	918	1	2	0	1846	2
CDKN2A	*21,967,753-21,995,301*	0	0	0	0	0	0	883	2
CDKN2B	*22,002,903-22,009,363*	0	0	0	0	0	0	62	2
CDKN2B-AS1	*21,994,778-22,121,097*	0	0	0	0	0	0	82	2
DMRTA1	*22,446,841-22,455,740*	0	0	0	1	0	1	0	2
ELAVL2	*23,690,104-23,826,337*	0	0	0	1	0	1	0	2
TUSC1	*25,676,389-25,678,440*	0	0	0	1	0	1	415	2
CAAP1	*26,840,685-26,892,804*	0	0	686	1	576	1	1307	2
PLAA	*26,904,083-26,947,463*	1	0	1411	1	1230	1	1939	2

Gene expression units are read counts / million (RCM). Regions of complete / near complete loss of expression and copy number (CN) of 0 are highlighted.

Figure Legends.

Figure 1. In Vivo and ex-vivo imaging of xenografts.

A. Serial quantification of luminescent signal from injected and contralateral femurs and the whole body for each xenograft suggesting variations in the rate at which cells migrate from the site of injection and the degree to which different sites are infiltrated by transduced cells. For example, in 3a/b^{SLIEW} the strength of signal from the contralateral femur lagged substantially behind that of the injected femur until weeks 10-13, while in 1a/b^{SLIEW} and 2b^{SLIEW}, the two femurs showed similar levels from week 2. **B**. Example of ex-vivo imaging of dissected organs showing total luminescent readings for spleen liver and kidney. Images are representative of six animals analysed. **C**. Examples of FACS analysis of cells isolated from the spleens of 3a^{SLIEW} and 4a^{SLIEW}, demonstrate marked contrast in the proportion of CD19+ve cells that are EGFP+ve. **D**. A single example of serial three dimensional reconstructions of luminescent signals in 2a^{SLIEW}, 11 and 15 weeks after transplant. Arrows point to regions of the skull, spleen and a third site showing strong signal increase between these two time points. The skeleton projected for orientation is not derived from this animal.

Figure 2. Histological sections of bone marrow from controls and xenograft transplanted with SLIEW transduced cells.

A. Control NSG mouse H&E stained femur showing heterogeneous cell types, abundant megakaryocytes and vascular structures. **B**. H&E stained femur from 4a^{SLIEW} showing tightly packed homogeneously stained cells and an absence of megakaryocytes and vascular structures (image representative of six animals showing only morphology type A) **C**. H&E stained femur from 3b^{SLIEW} showing heterogeneous cell types but in comparison with controls; loss of cellularity and organisation, absence of vascular structures, reduced numbers of megakaryocytes and presence of small darkly stained cells or cellular fragments (image representative of two animals showing

morphology type B) **D**. The only example seen of co-existence of A and B type morphology in a sternum segment of $3b^{SLIEW}$: 1st left panel; H&E stained whole section with box marking the region shown in the 2nd left panel. 2nd left panel; H&E stained detail of a single sternum segment displaying both A and B type morphologies. Middle panel; whole sections stained with anti-human CD19 and Ki-67 antibodies, arrowheads indicate three regions corresponding to high resolution images in the right hand panels. Right hand panels; high resolution images of anti-CD19 and Ki-67 staining from regions 1, 2 and 3. Anti-CD19 and Ki67 stained human leukemia cells remain tightly packed (region 2) with little diffusion to adjacent areas of acellular marrow (region 3). Anti-Ki67 and CD19 staining demonstrating that the proportion of cycling human cells are reduced in region 2 compared with region 1 suggesting a microenvironment less favourable for leukemia cell growth. **E**. Examples of TEM images of xenograft tibia sections. In $4a^{SLIEW}$ and $1a^{SLIEW}$ cells appear homogeneous compared with controls (Supplementary Figure 6) and have a high nuclear to cytoplasmic ratio (VL morphology). $3a^{SLIEW}$ and $2a^{SLIEW}$ displaying evidence for cell death and characteristics of apoptosis, such as chromatin clumping and nuclear fragmentation (AP morphology). Images are representative of four animals each showing VL and AP morphology. **F**. Examples of skull and brain sections from $3b^{SLIEW}$ (left panel) and $1b^{SLIEW}$ (right panel) showing heavy infiltration of the calvaria in both cases (arrow 1), light ($3b^{SLIEW}$) and heavy ($1b^{SLIEW}$) infiltration of the meninges, respectively (arrow 2). Images are representative of seven animals. **G**. Two examples of H&E stained patient trephines. The left hand panel is from patient 1 for comparison with the leukemia cells from the same patient in a mouse ($1a^{SLIEW}$) tibia section shown in **B.** Images are representative of seven iAMP21-ALL patient trephines analysed. Scale bars are; **A**, **B**, **C**, two right hand panels of **D** and **G** - 50 µm, far left hand and two middle panels of **D** – 1 mm, second from left panel of **D** and **F** 200µm and **E** - 10µm.

Figure 3. Analysis of CNA evolution in xenografts models.

Panels in blue boxes show heat maps of copy number from SNP6.0 arrays for chromosomal regions showing evidence of clonal genomic evolution in xenografts, P (presentation), R (remission), 1°,2° and 3° (primary, secondary and tertiary xenografts). Box-flow diagrams illustrate loss, gain or change

in level of genomic abnormalities. White boxes; sample analysed, grey boxes; sample not analysed, red type; CN gain of one, purple; CN gain of two, light red; sub-clonal CN gain, black; CN loss of one, blue; CN loss of two, grey; sub-clonal loss, green CN-LOH. * indicates deletion was detected by whole genome sequencing but not by SNP6.0 array. **A**. Patient 1 – including heat maps of 9p demonstrating gain of bi-allelic deletion of a region containing *CDKN2A/B* and focal mono-allelic deletion of a region of 3p containing the *CMTM* genes 6-8. Chromosome 21 heat maps illustrate a complex pattern of copy number gain and loss characteristic of iAMP21 and also demonstrate additional CN changes in one 2° and all 3° xenografts. The colour coded bar depicts regions of chromosome loss or gain in the derivative iAMP21, [der(iAMP21)]. Green box; chromosome 21 CN profiles before and after iAMP21 evolution and showing the position of probes used for FISH analysis. Upper black box; FISH image of metaphase and interphase cells showing multiple copies of the *RUNX1* region and 3 copies of the *APP* region at presentation. Lower black box; FISH images showing three or one copy of the *APP* region in cells from the patient, a 1° and two 2° xenografts. **B.** CNAs discordant between patient 2 and xenografts including; loss of whole chromosome (WC) X, gain of an iso(Xp) and gain of a focal deletion of Xp involving the genes *ZNF157* and *ZNF41*. **C**. CNA discordant between patient 3 and xenografts including different deletions involving *ETV6* one of which potentially resulted in a novel *ETV6-BICD1* fusion gene. **D.** Differences in copy number profiles between three 1° xenografts from patient 4. These included two different large mono-allelic deletions of chromosome 10 (1 and 2) both of which contained a focal bi-allelic deletion (3), present in all xenografts and involving *PIK3AP1* and *LCOR*. A second bi-allelic deletion (4) was present in two xenografts only and involved *BLNK*. Other discordant CNA included complex rearrangements of 17q and 14q, focal deletions of 4q34.1, 16p13 and 22q13.1 and a focal amplification of 4q13.2. **E.** Sub-clonal deletions at 2p25.1, 3q13.3 and 12q24.1 present in patient 5 became dominant clones in the xenograft while a sub-clonal deletion of 3p21.3 was lost and sub-clonal deletions of 1q42.3 and 5q33.3 (marked by red arrow 1) were gained. In the patient relapse sample the 3p21.3 deletion became dominant while other sub-clonal abnormalities detected at presentation were lost. As with the xenograft a focal deletion of 5q33.1

(marked by red arrow 2) emerged at relapse. The two 5q deletions both resulted in loss of coding exons of *EBF1*. Genomic positions of breakpoints derived from SNP6.0 analysis and genes contained within focal CNA, for all patient and xenografts, are annotated in Supplementary Table 7.

Figure 4. Analysis of mutations affecting the RAS pathway. Key for analytical methods used are shown top right. Blue boxes show non-synonymous RAS pathway mutations identified. White boxes summarise the estimated variant allele (VA) frequencies and methods of analysis used for patient and xenograft samples. **A**) In patient 1 an NF1 mutation was clonal at presentation and in all xenografts. By contrast mutations of NRAS and KRAS showed marked fluctuations in VA frequency; NRAS (1), present in the patient as a sub-clone, was detected in both 1° xenografts but not in blasts from 2° and 3° animals. NRAS (2), identified by high depth targeted sequencing in 1% of patient sample reads, was undetected by whole exome sequencing in primografts but emerged as a dominant clone in 2°2a and all derivative 3° xenografts. A mutation of KRAS, although undetected in more than 6000 reads by targeted sequencing of the patient sample, marked the dominant clone present in primografts and 2°2b. Sanger sequence traces illustrate the relationship between the NF1, NRAS (2) and KRAS mutations in the two 2° xenografts, traces shown for 2°1a are also representative of 1°1a and 1°1b, traces shown for 2°1b are also representative for 3°1a-g. **B**) In patient 3 an NRAS mutation identified in the patient remained clonal in all 1° and 2° xenografts. The Sanger sequencing trace shown for 1°3a is representative of all xenografts. **C**) In patient 5 a FLT3 itd, detected as a minor sub-clone by exome sequencing of the presentation sample, became dominant in the 1° xenograft as demonstrated by the generation two distinct exon 14 PCR amplicons of equal intensity (first lane bottom right). In contrast only a single PCR product was amplified from the relapse sample of this patient (second lane bottom right). Mutations detected in patient presentation samples have been previously published.(13)

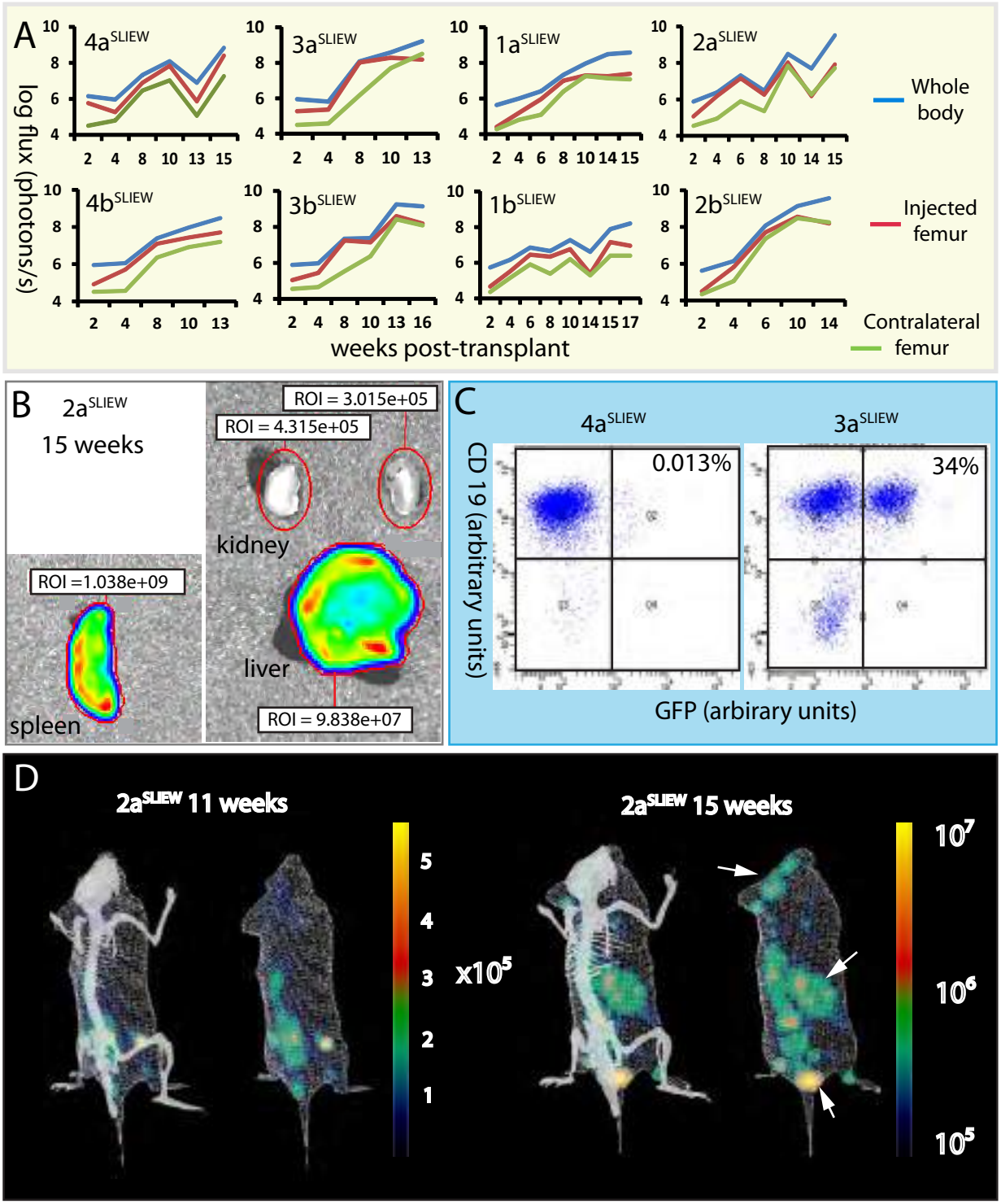
A
4a SLIEW
3a SLIEW
1a SLIEW
2a SLIEW
4b SLIEW
3b SLIEW
1b SLIEW
2b SLIEW
log flux (photons/s)
weeks post-transplant
Whole body
Injected femur
Contralateral femur
B
2a SLIEW
15 weeks
ROI = 3.015e+05
ROI = 4.315e+05
kidney
ROI =1.038e+09
liver
spleen
ROI = 9.838e+07
C
4a SLIEW
3a SLIEW
0.013%
34%
CD 19 (arbitrary units)
GFP (arbirary units)
D
2a SLIEW 11 weeks
2a SLIEW 15 weeks
x10^5
10^7
10^6
10^5

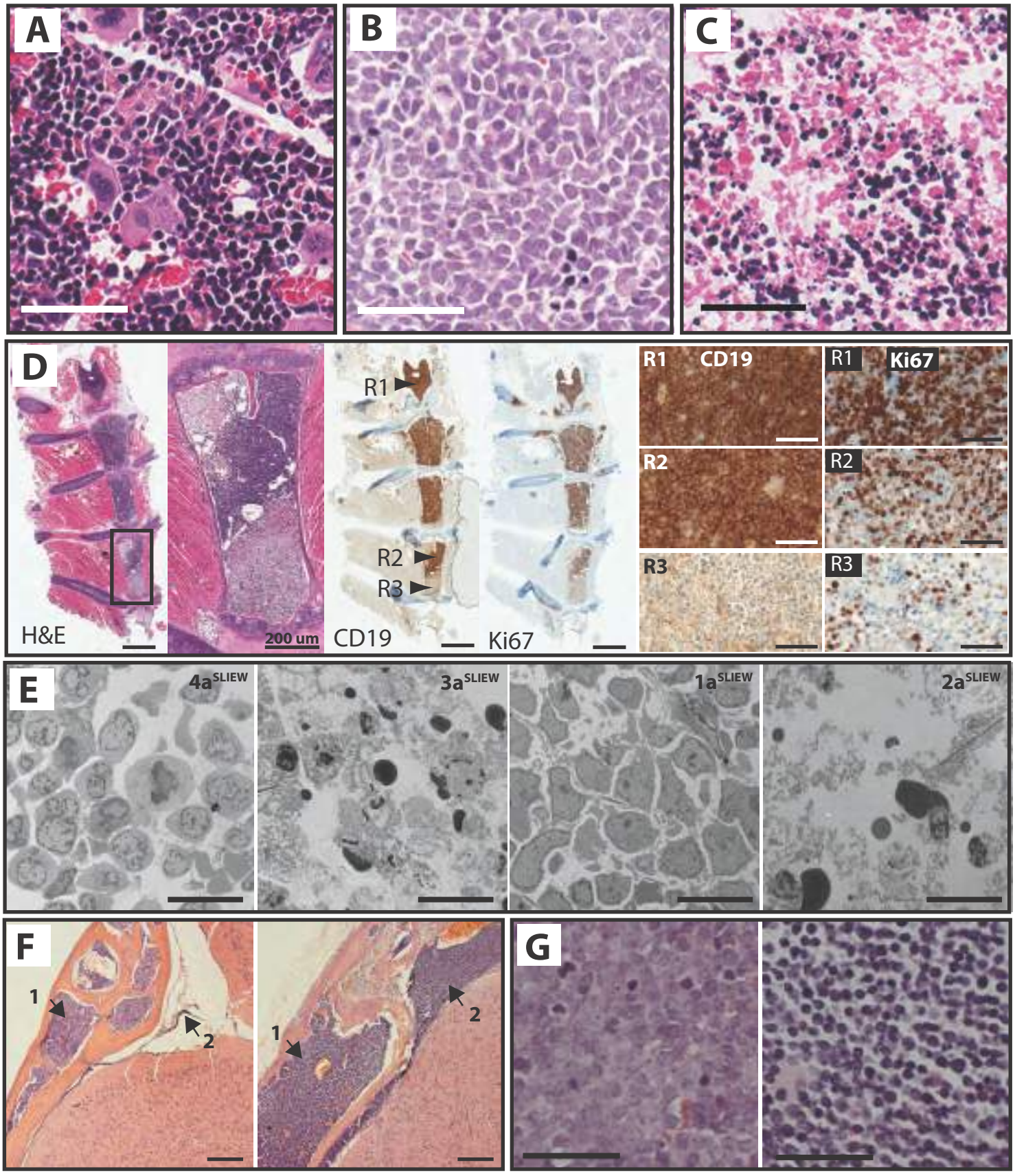
A
B
C
D
H&E
200 um
R1
R2
R3
CD19
Ki67
R1 CD19
R1 Ki67
R2
R2
R3
R3
E
4a SLIEW
3a SLIEW
1a SLIEW
2a SLIEW
F
1
2
1
2
G

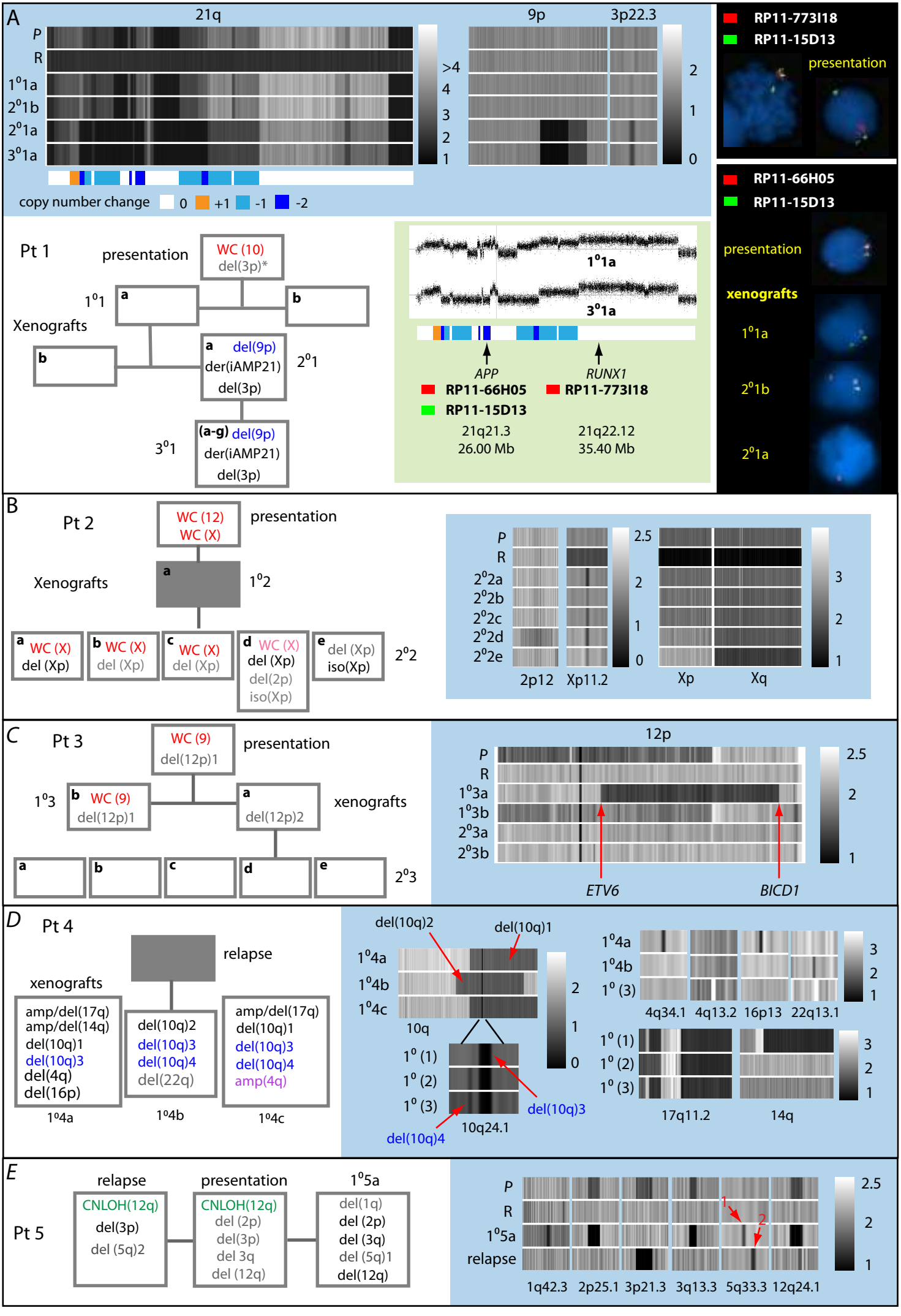
A
21q
9p
3p22.3
P
R
1°1a
2°1b
2°1a
3°1a
>4
4
3
2
1
2
1
0
copy number change
0
+1
-1
-2
RP11-773I18
RP11-15D13
presentation
RP11-66H05
RP11-15D13
presentation
xenografts
1°1a
2°1b
2°1a
Pt 1
presentation
WC (10)
del(3p)*
1°1
a
b
Xenografts
b
a del(9p)
der(iAMP21)
del(3p)
2°1
3°1
(a-g) del(9p)
der(iAMP21)
del(3p)
1°1a
3°1a
APP
RUNX1
RP11-66H05
RP11-773I18
RP11-15D13
21q21.3
26.00 Mb
21q22.12
35.40 Mb
B
Pt 2
WC (12)
WC (X)
presentation
Xenografts
a
1°2
a WC (X)
del (Xp)
b WC (X)
del (Xp)
c WC (X)
del (Xp)
d WC (X)
del (Xp)
del(2p)
iso(Xp)
e del (Xp)
iso(Xp)
2°2
P
R
2°2a
2°2b
2°2c
2°2d
2°2e
2.5
2
1
0
3
2
1
2p12
Xp11.2
Xp
Xq
C
Pt 3
WC (9)
del(12p)1
presentation
1°3
b WC (9)
del(12p)1
a
del(12p)2
xenografts
a
b
c
d
e
2°3
12p
P
R
1°3a
1°3b
2°3a
2°3b
2.5
2
1
ETV6
BICD1
D
Pt 4
relapse
xenografts
amp/del(17q)
amp/del(14q)
del(10q)1
del(10q)3
del(4q)
del(16p)
1°4a
del(10q)2
del(10q)3
del(10q)4
del(22q)
1°4b
amp/del(17q)
del(10q)1
del(10q)3
del(10q)4
amp(4q)
1°4c
del(10q)2
del(10q)1
1°4a
1°4b
1°4c
2
1
0
10q
1° (1)
1° (2)
1° (3)
del(10q)3
del(10q)4
10q24.1
1°4a
1°4b
1° (3)
3
2
1
4q34.1
4q13.2
16p13
22q13.1
1° (1)
1° (2)
1° (3)
3
2
1
17q11.2
14q
E
Pt 5
relapse
CNLOH(12q)
del(3p)
del (5q)2
presentation
CNLOH(12q)
del (2p)
del(3p)
del 3q
del (12q)
1°5a
del(1q)
del (2p)
del (3q)
del (5q)1
del(12q)
P
R
1°5a
relapse
1
2
2.5
2
1
1q42.3
2p25.1
3p21.3
3q13.3
5q33.3
12q24.1

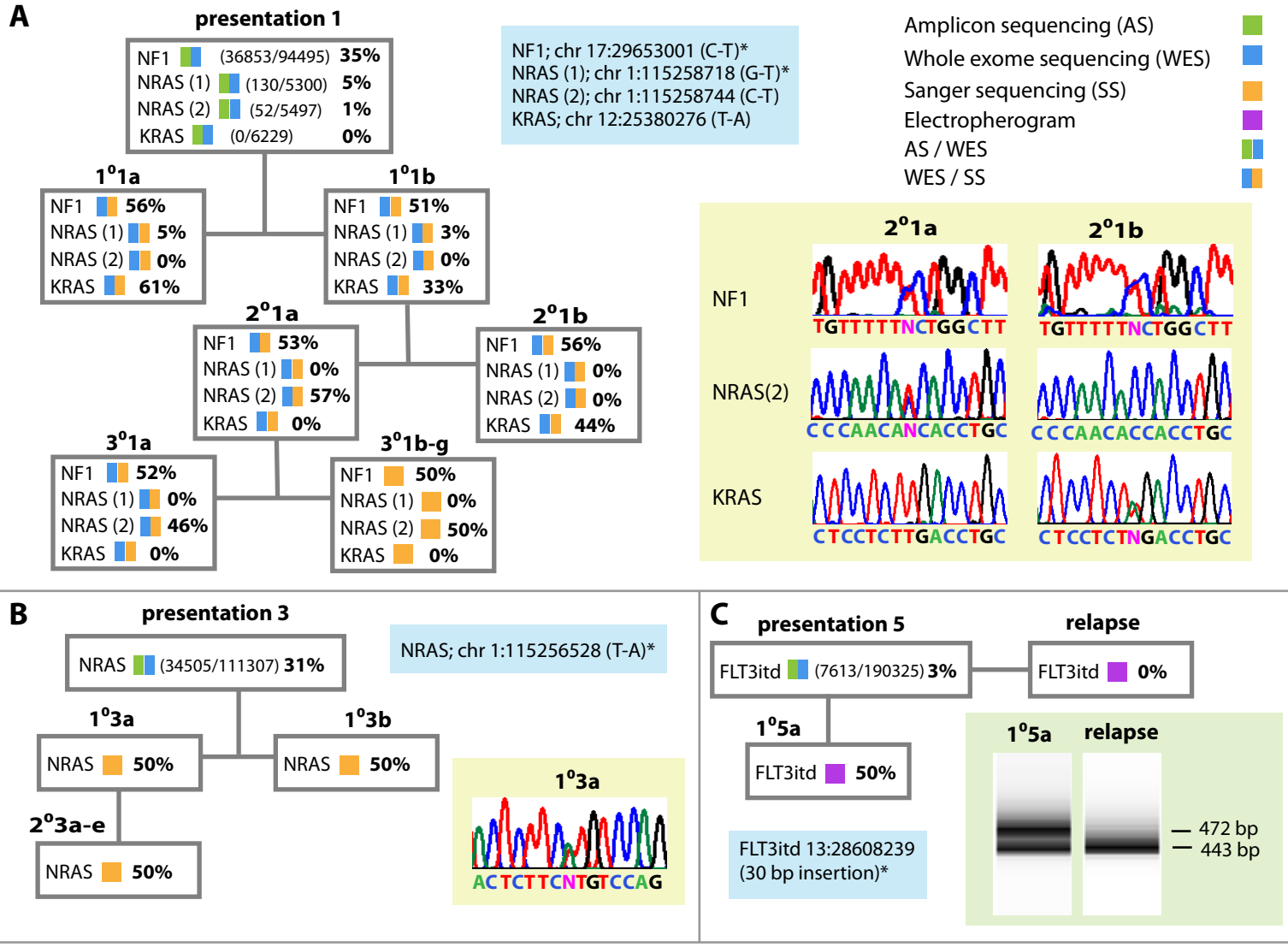
A
presentation 1
NF1 (36853/94495) 35%
NRAS (1) (130/5300) 5%
NRAS (2) (52/5497) 1%
KRAS (0/6229) 0%
1°1a
NF1 56%
NRAS (1) 5%
NRAS (2) 0%
KRAS 61%
1°1b
NF1 51%
NRAS (1) 3%
NRAS (2) 0%
KRAS 33%
2°1a
NF1 53%
NRAS (1) 0%
NRAS (2) 57%
KRAS 0%
2°1b
NF1 56%
NRAS (1) 0%
NRAS (2) 0%
KRAS 44%
3°1a
NF1 52%
NRAS (1) 0%
NRAS (2) 46%
KRAS 0%
3°1b-g
NF1 50%
NRAS (1) 0%
NRAS (2) 50%
KRAS 0%
NF1; chr 17:29653001 (C-T)*
NRAS (1); chr 1:115258718 (G-T)*
NRAS (2); chr 1:115258744 (C-T)
KRAS; chr 12:25380276 (T-A)
Amplicon sequencing (AS)
Whole exome sequencing (WES)
Sanger sequencing (SS)
Electropherogram
AS / WES
WES / SS
2°1a
2°1b
NF1
NRAS(2)
KRAS
TGTTTTTNCTGGCTT
CCCAACANCACCTGC
CTCCTCTTGACCTGC
TGTTTTTNCTGGCTT
CCCAACACCACCTGC
CTCCTCTNGACCTGC

B
presentation 3
NRAS (34505/111307) 31%
1°3a
NRAS 50%
1°3b
NRAS 50%
2°3a-e
NRAS 50%
NRAS; chr 1:115256528 (T-A)*
1°3a
ACTCTTCNTGTCCAG

C
presentation 5
FLT3itd (7613/190325) 3%
1°5a
FLT3itd 50%
relapse
FLT3itd 0%
FLT3itd 13:28608239
(30 bp insertion)*
1°5a
relapse
472 bp
443 bp

Supplementary methods

Determination of xenograft experimental end points. Mice were checked daily for signs of ill health and routinely weighed once a week or more often if indicated. Mice were culled at end stage disease as defined by; weight gain of >20%, weight loss reaching 20% at any time or >10% maintained for 72 hours compared with weight at the start of the experiment, starey coat, porphyrin staining of eyes and nose or sunken eyes, persistent skin tenting, immobility, unresponsive or very aggressive behaviour, loss of upright stance, laboured respiration, blood staining or other discharge, signs of anaemia including extreme paleness of feet, tail and ears.

Immunophenotyping of xenografts cells. Proportions of human and mouse cells were determined by flow cytometry using anti-human CD10 FITC or CD19 PE in combination with anti-murine-CD45, PE-Cy7 and anti-TER119 PE-Cy7, as previously described.(1) Selected xenografts were further characterised using a panel of anti-human CD19-APC, CD10-PE, CD34-Cy5.5 and CD38-FITC together with anti-mouse CD45-Cy7-A. Cells were initially gated on a lymphocyte population defined by forward and side scatter and on the anti-mouse CD45 negative population. For each sample, identical markers were used to divide the gated cells into human CD19, CD10, CD45 and CD38 negative and positive populations based on median fluorescence intensity (MFI) of the unstained cells. MFI and % positive cells (supplementary table 5) refer to the total gated population with the exception of a minority of samples where the proportion of cells staining positively for mouse CD45 was high and a significant proportion of gated cells, negative for all human markers, was assumed to be of mouse origin and gated out. All antibodies were obtained from BD Biosciences (Oxford, UK) and stained cells were analysed with a BD FACSCanto II cell analyser and processed with FlowJo (Oregon, USA) software .

Lentiviral transduction, In-vitro culture and in-vitro, in-vivo and ex-vivo imaging of xenograft cells. SLIEW lentivirus was produced as previously described(1) with the modification that HEK293FT cells (Thermo Fisher Scientific) and EndoFectin (GeneCopoeia) transfection reagent were used. Lentiviral stocks were concentrated by ultracentrifugation for 2 hours at an RCF of 83018 and re-suspended in Serum free expansion medium (SFEM) (Stemcell Technologies) supplemented with 10% FCS before titrating in 293FT cells. For each patient analysed, $1.2x10^7$ xenograft cells in SFEM supplemented with 10% FCS and 10ng/ml IL-7, were transduced at a multiplicity of infection of 1.0 in delta T25 tissue culture flasks. Following overnight incubation medium was replaced and approximately 72 hours after transduction $0.5x10^6$ cells were analysed for EGFP expression by FACS, $1.5x10^6$ cells were transplanted into each of two NSG mice and $6x10^6$ cells were re-suspended in αMEM with 10% FCS for in-vitro co-culture. Co-cultures were established by plating $2x10^6$ transduced xenograft cells in

1ml of medium on MS-5 cells (DSMZ # ACC441) (83,000 cells plated /well in 12 well plates) that had been irradiated with 50 Gy 24hrs after plating. EGFP expression of co-cultured cells was assessed using an EVOS fluorescent inverted microscope (Life technologies). 2D and 3D bioluminescent whole body imaging of mice transplanted with transduced xenograft cells was performed with an IVIS Spectrum (Caliper Life Sciences, Hopkington, MA, USA) 10 minutes after intraperitoneal injection of 100ul of D-luciferin (30mg/ml, VivoGlo, Promega). Immediately following final whole body imaging mice were killed and organs dissected and imaged ex-vivo. Quantification of luminescent signals and 3D reconstructions were performed using Living image version 4.3.1 software (Caliper Life Sciences). The proportion of leukaemia cells expressing SLIEW in spleen preparations was measured by immunostaining and FACS by determining numbers of EGFP+ve cells in the human CD19+ve and / or CD10+ve, murine CD45 / TER119 –ve population.

Histopathology.

After transfer to 10% neutral buffered formalin immediately after dissection, tibias and sternums were decalcified, paraffin embedded, sectioned and stained with haematoxylin and eosin (H&E) or human antibodies, according to standard histopathological techniques, by the department of Cellular Pathology, Newcastle upon Tyne Hospitals NHS Foundation Trust. Mouse heads preserved in formalin were sectioned and stained as previously described.(2)

Transmission Electron Microscopy (TEM). TEM was performed by the Electron Microscopy Unit, Faculty of Medical Sciences, Newcastle University. Small trephines of bone were fixed in 5% glutaraldehyde in 3% PFA in phosphate buffer overnight. Samples were then rinsed in phosphate buffer before being placed in EDTA for a minimum of 24hrs at 40^{O}C. After rinsing in phosphate buffer the samples were placed in 1% osmium tetroxide for 2hrs at RT. They were then rinsed in buffer, dehydrated through a graded series of acetone and embedded in TAAB epoxy resin (medium). After polymerisation at 60^{O}C the samples were sectioned on an ultramicrotome and ultrathin sections (70nm) were picked up on copper grids, stained with uranyl acetate and lead citrate and viewed on a Philips CM100 TEM at 100kV.

RNA Sequencing.

RNA was extracted from cells isolated from xenograft spleens and purified over Ficol using an RNeasy kit (Qiagen). Illumina RNA sequencing was performed by Aros Applied Biotechnology, Eurofins Genomics Group, Aarhus, DK.

Analysis of RAS pathway mutations. Whole exome sequencing (WES) was performed on selected xenografts derived from patient 1 using library preparation and sequencing techniques as previously

described(3). To filter mouse sequences from xenograft samples, the programme, Xenome v 1.0.1, was used to simultaneously align reads to version GRCm38 and hg19 of the mouse and human genomes, respectively(4). Default settings of xenome index and classify were used to designate reads as of human or mouse origin, ambiguous, both or neither, with only unambiguous human reads used for subsequent analysis. Reads were aligned using Burrows-Wheeler Aligner (BWA) version 0.7.12.(5, 6) and MuTect1.7 (7) was used for calling somatic single nucleotide variants (SNVs) following Broad Best practices(8, 9). Calls were derived from jointly realigned and recalibrated tumour normal (patient remission sample) BAM files and annotated with ENSEMBL Variant Effect Predictor (VEP) version 83(10). Patient BAM files were re-analysed manually in Integrated Genome Viewer(11) to assess levels of SNV affecting the RAS pathway, predicted to have an oncogenic role (mutations located within coding regions and predicted to affect protein function using SIFT, Polyphen2 and Mutation Taster) and identified by WES in xenografts but not previously in the patient (KRAS, chr12:25380276, T->A; NRAS, chr1:115258744, C->T).

To validate clonal SNV affecting *NF1*, *NRAS* and *KRAS* and extend analysis to remaining patient 1 xenografts, affected exons were amplified and analysed by sanger-sequencing (Durham Genome Centre, Durham UK). Sequence traces were examined manually using FinchTV (Information Technologies, Inc, MO, USA). Target sequence amplification and Sanger-sequencing was also used to analyse an NRAS mutation in xenografts, previously identified in patient 3. Levels of a *FLT3* 30 nucleotide internal tandem duplication (ITD) identified in patient 5 were assessed in xenografts and a relapse sample using targeted sequencing in combination with electrophoretic analysis of amplicon size using a 2100 Bioanalyzer (Agilent technologies, CA USA). All primer sequences used for exon amplification have been previously published (3).

Supplementary Figures

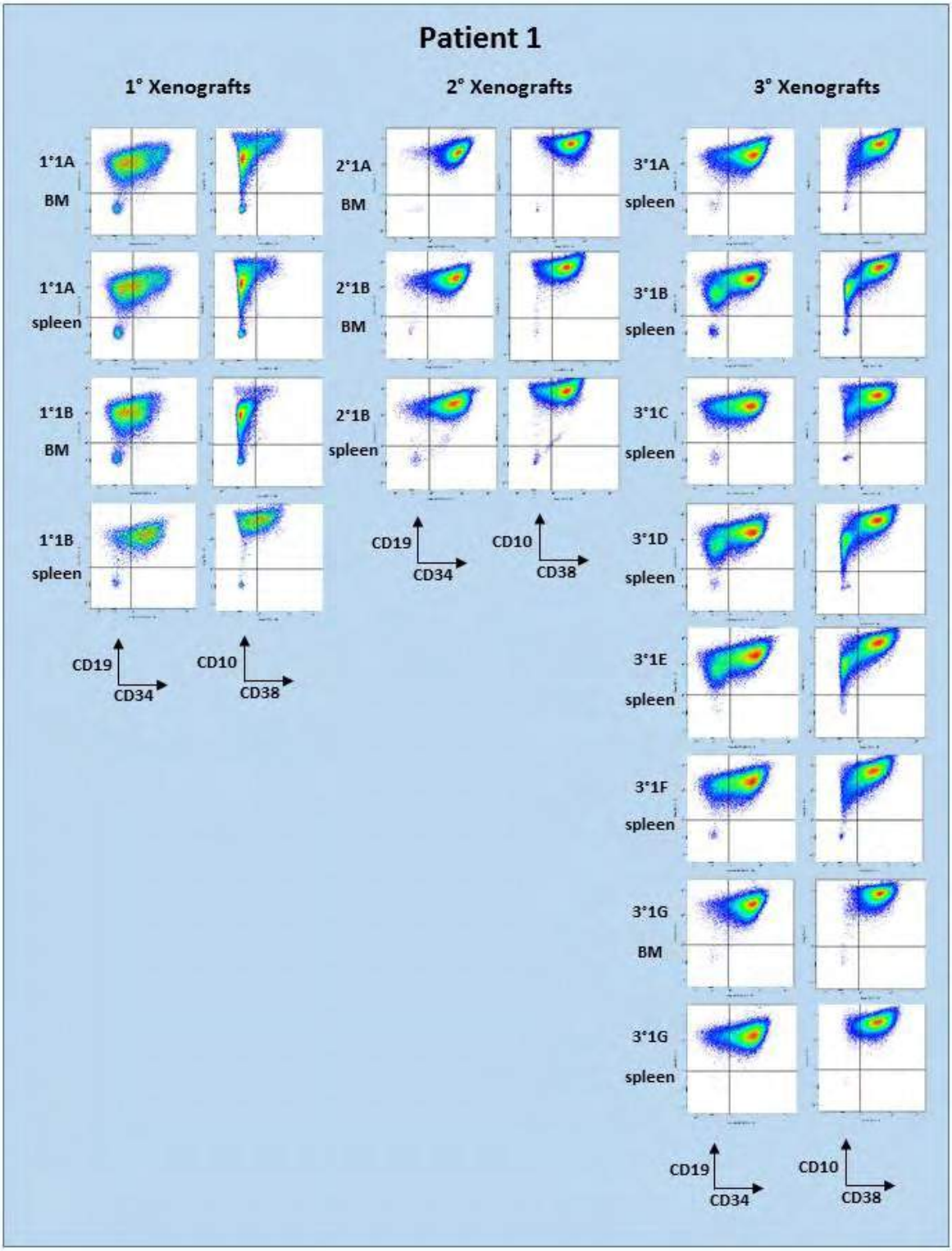

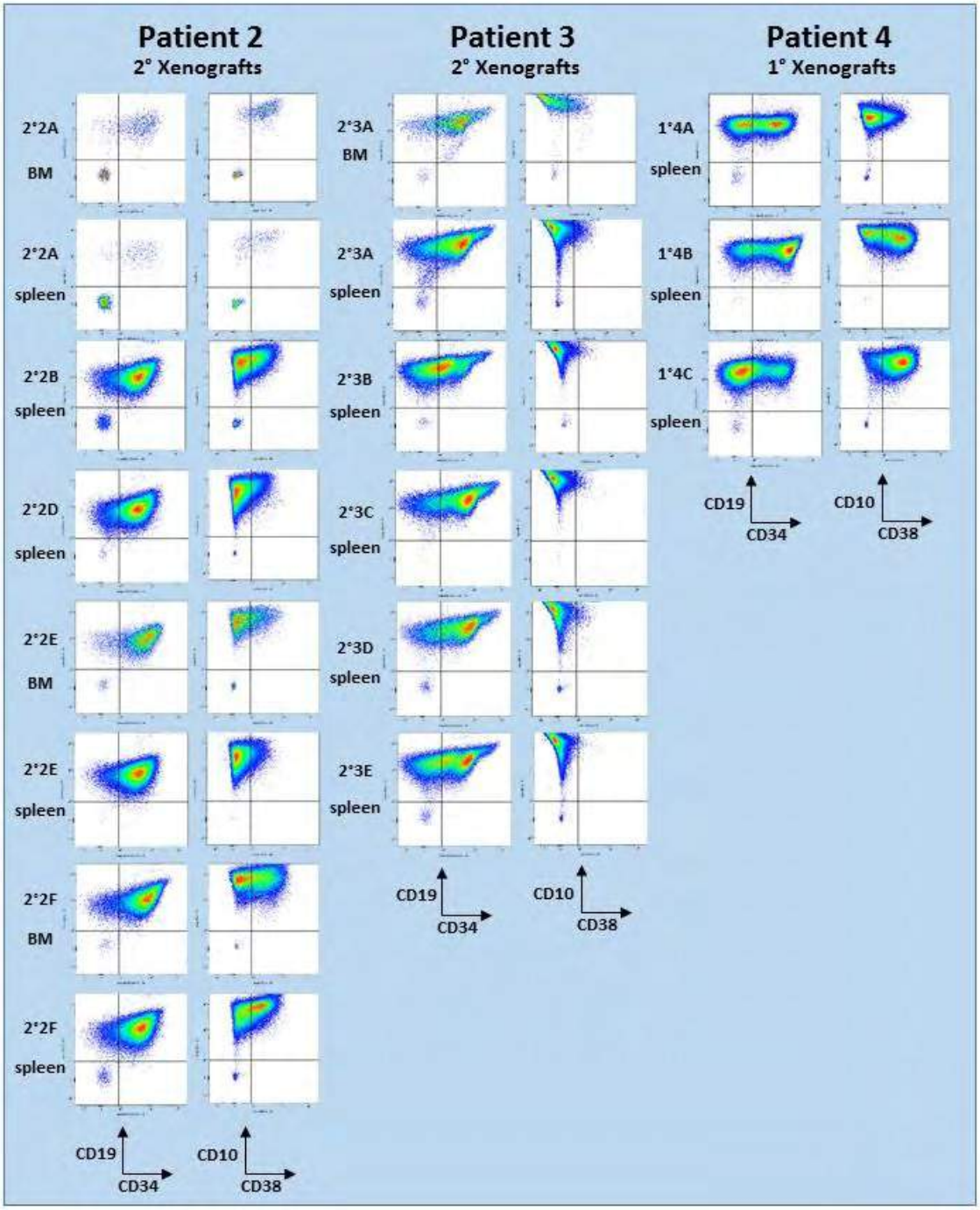

Supplementary Figure 1. FACS analysis demonstrates immunophenotypic heterogeneity between xenografts. Expression of CD19, CD34, CD10 and CD38 are shown for bone marrow (BM) and / or spleen samples for xenografts from patients 1-4 as indicated. Scales are bi-exponential and units are arbitrary.

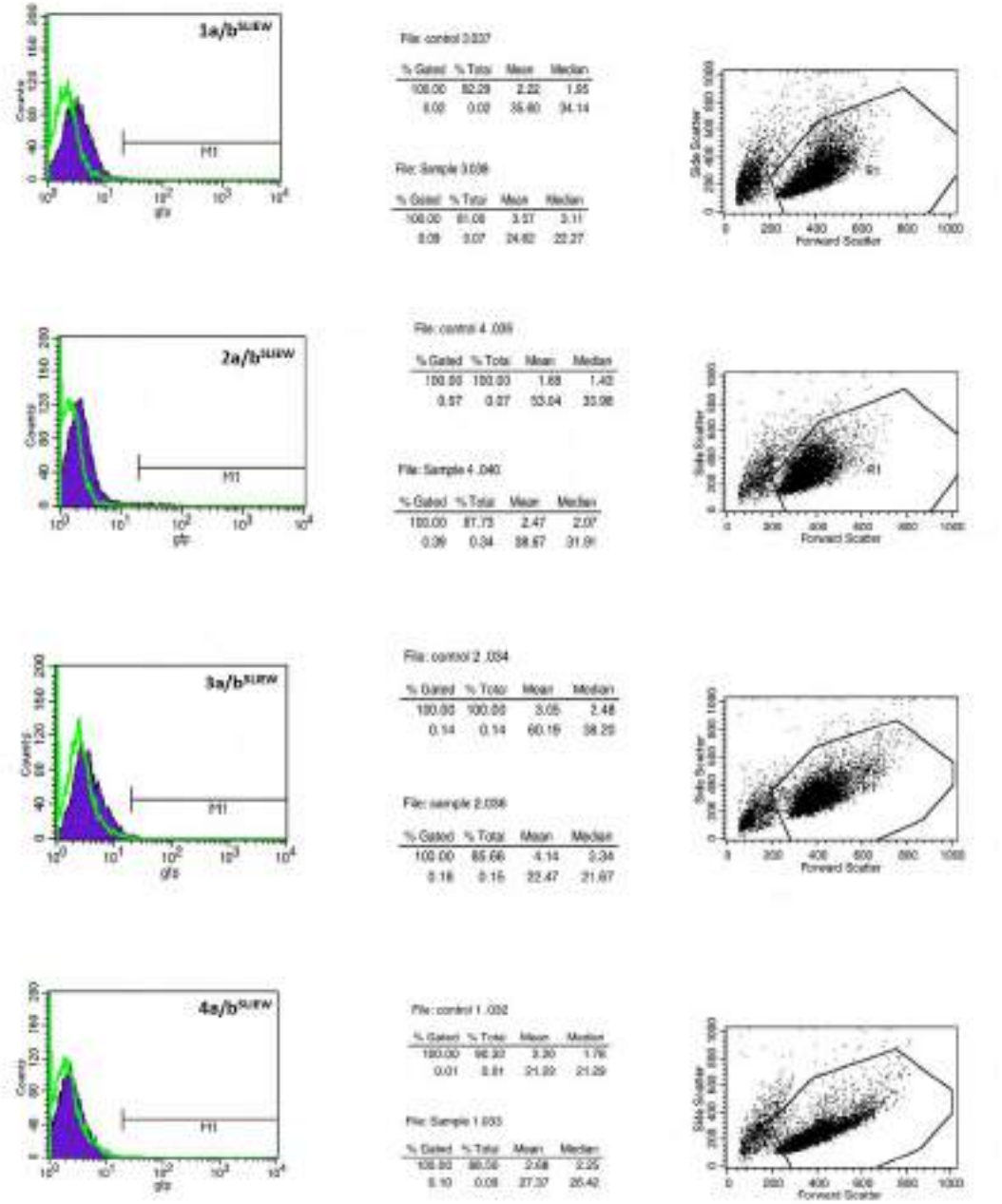

Supplementary figure 2. FACS analysis of iAMP21-ALL cells isolated from xenografts transduced with SLIEW lentivirus prior to transplant. FACS plots showing levels of EGFP expression (arbitrary units) in control (green trace) or transduced cells (purple infill). Live cells were gated on forward and side scatter as shown in the right hand box. In all cases the proportion of cells with GFP levels outside the control range (marker by M1) were less than 1%.

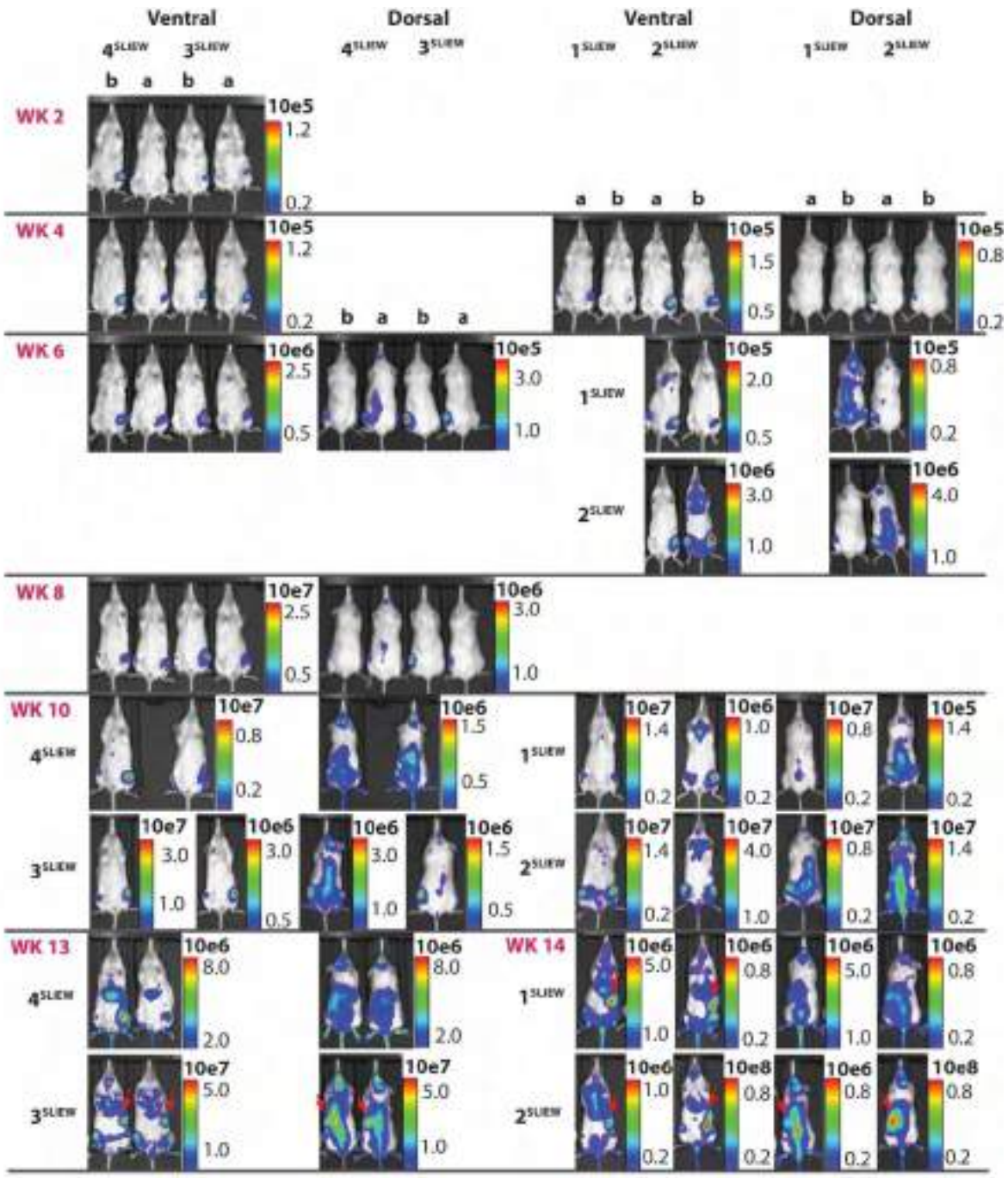

Supplementary Figure 3. Serial bioluminescent imaging of all NSG mice transplanted with pSLIEW transduced iAMP21-ALL xenograft derived cells. Measurement of luciferase activity demonstrates variation in the rate of spread of leukaemia from the site of injection to other bones and organs. Spleen involvement (marked by red arrows) was most obvious in $1a^{SLIEW}$ $1b^{SLIEW}$, $2a^{SLIEW}$and $2b^{SLIEW}$ but undetectable in $4a/b^{SLIEW}$. All captured images are shown. Scale is radiance (p/sec/cm^2/sr).

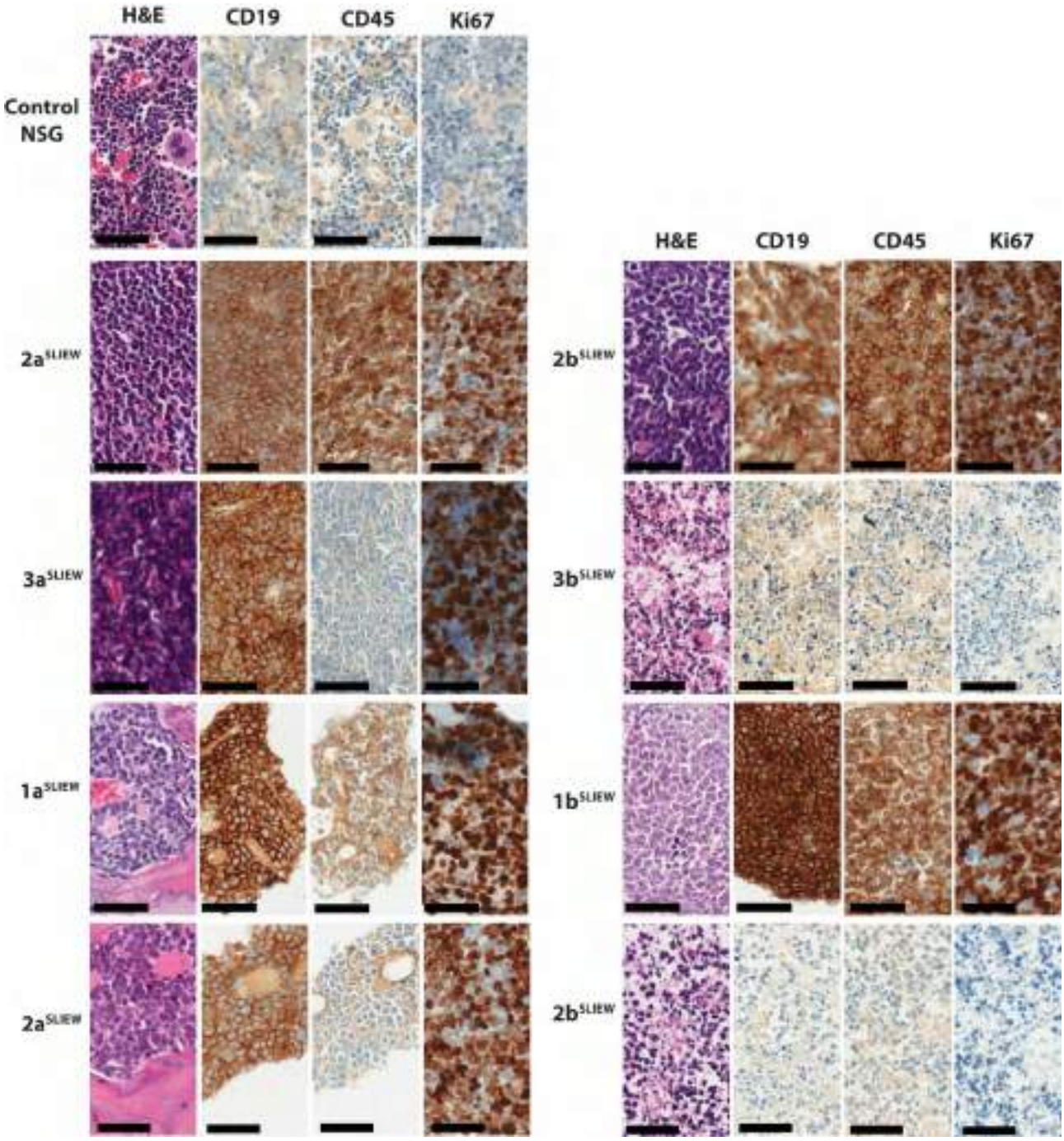

Supplementary Figure 4. Histological sections of control and SLIEW transduced iAMP21-ALL xenograft bone marrows.

Sections of NSG control and xenograft mouse tibias stained with H&E and anti-human CD19, CD45 and Ki67. 4a^{SLIEW}, 4b^{SLIEW}, 3a^{SLIEW}, 1a^{SLIEW}, 1b^{SLIEW} and 2a^{SLIEW} have packed homogeneous cells similar to those seen in iAMP21-ALL patient trephines (Figure 2G and Supplementary Figure 5), that stain positively for human CD19 and Ki67 and for CD45 in 4a^{SLIEW}, 4b^{SLIEW}, 1a^{SLIEW} and 1b^{SLIEW} only (morphology type A). 3b^{SLIEW} and 2b^{SLIEW} show loss of cellularity and evidence for apoptosis and stain negatively for CD19, CD45 and Ki67 (morphology type B). In each case the image shown is representative of all bone marrow in the section analysed. Scale bars are 50µm.

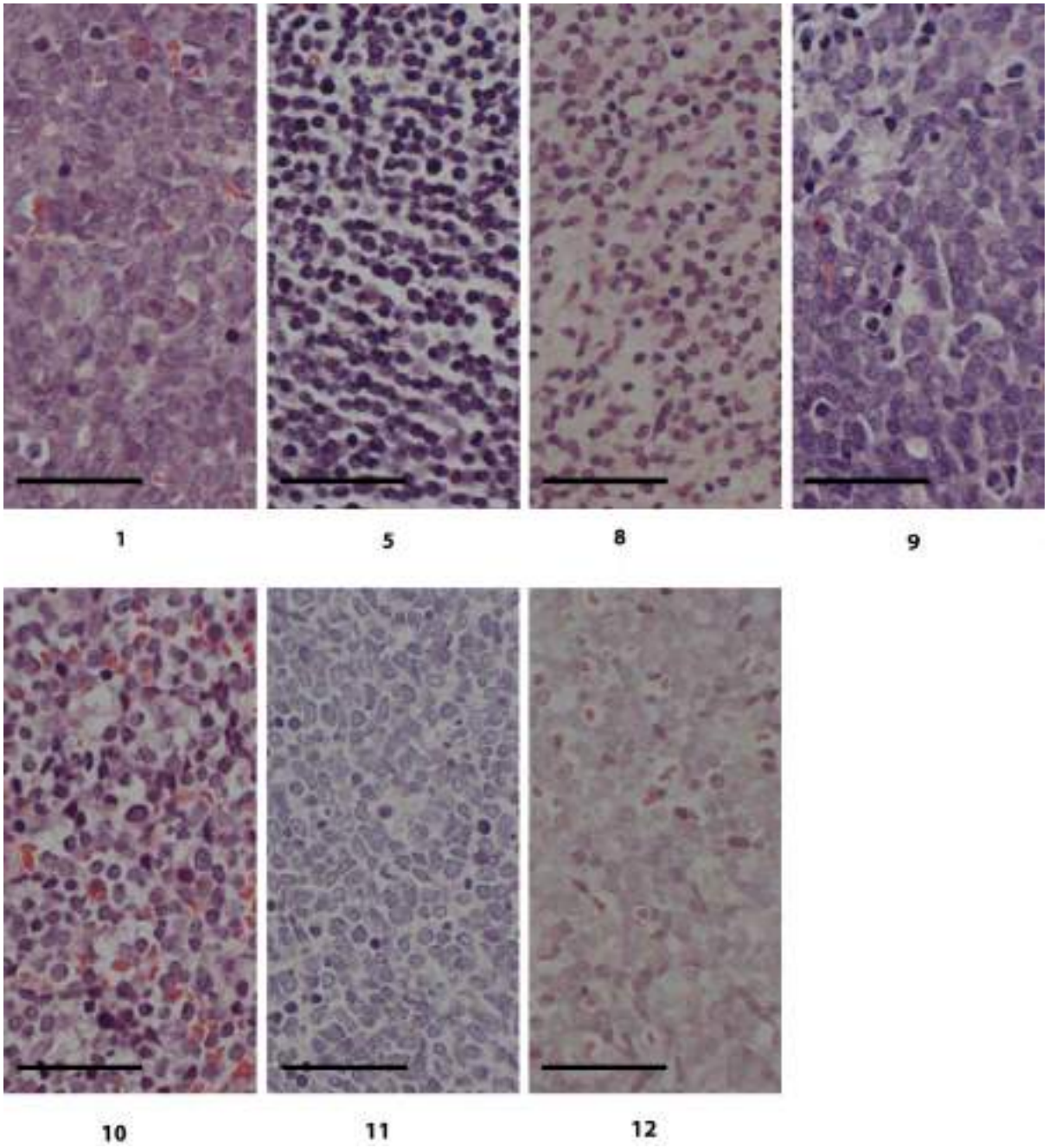

Supplementary Figure 5. iAMP21-ALL patient trephines. H&E stained sections through iAMP21-ALL trephine sections showing morphology similar to that of xenograft type A (Figure 2 and Supplementary Figure 4) with packed homogeneous cells and loss of vasculature and megakaryocytes. Patient karyotypes and demographic details are provided in supplementary table 2. In each case the image shown is representative of all bone marrow in the trephine section. Scale bars are 50µm.

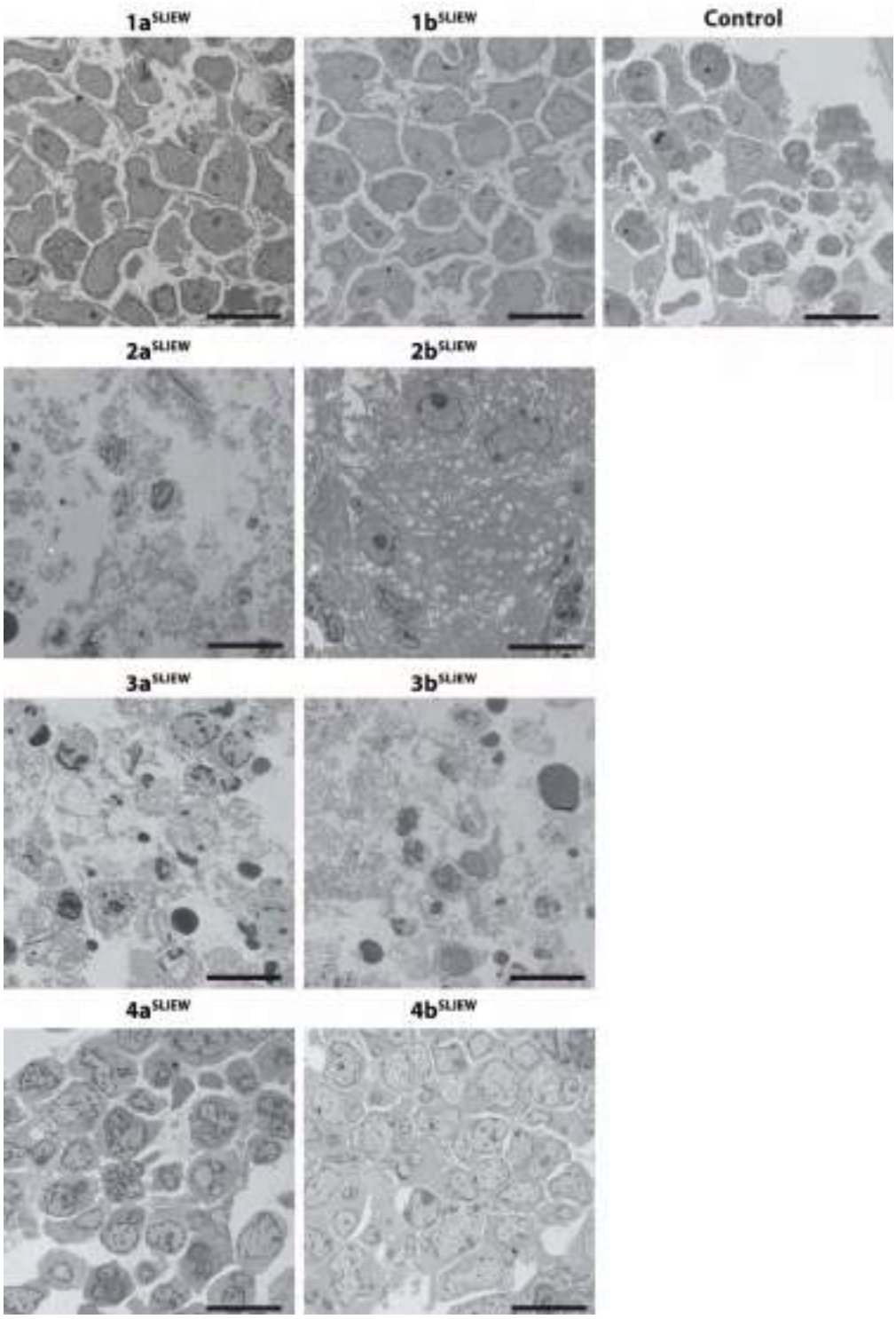

Supplementary Figure 6. Transmission electron microscopy (TEM) of control and SLIEW transduced iAMP21-ALL xenograft bone marrows.

TEM of ultra-thin sections of xenograft bone marrow; $4a^{SLIEW}$, $4b^{SLIEW}$, $1a^{SLIEW}$ and $1b^{SLIEW}$ have homogeneous cells with high nuclear to cytoplasmic ratio (VL morphology), compared with the control section, they lack vascular structures and cellular heterogeneity. $2a^{SLIEW}$, $2b^{SLIEW}$, $3a^{SLIEW}$ and $3b^{SLIEW}$ show loss of cellularity and evidence for apoptosis, such as chromatin clumping and nuclear fragmentation (AP morphology). Each image is representative of 6 regions captured from a single tibia section. Scale bars are 10µm.

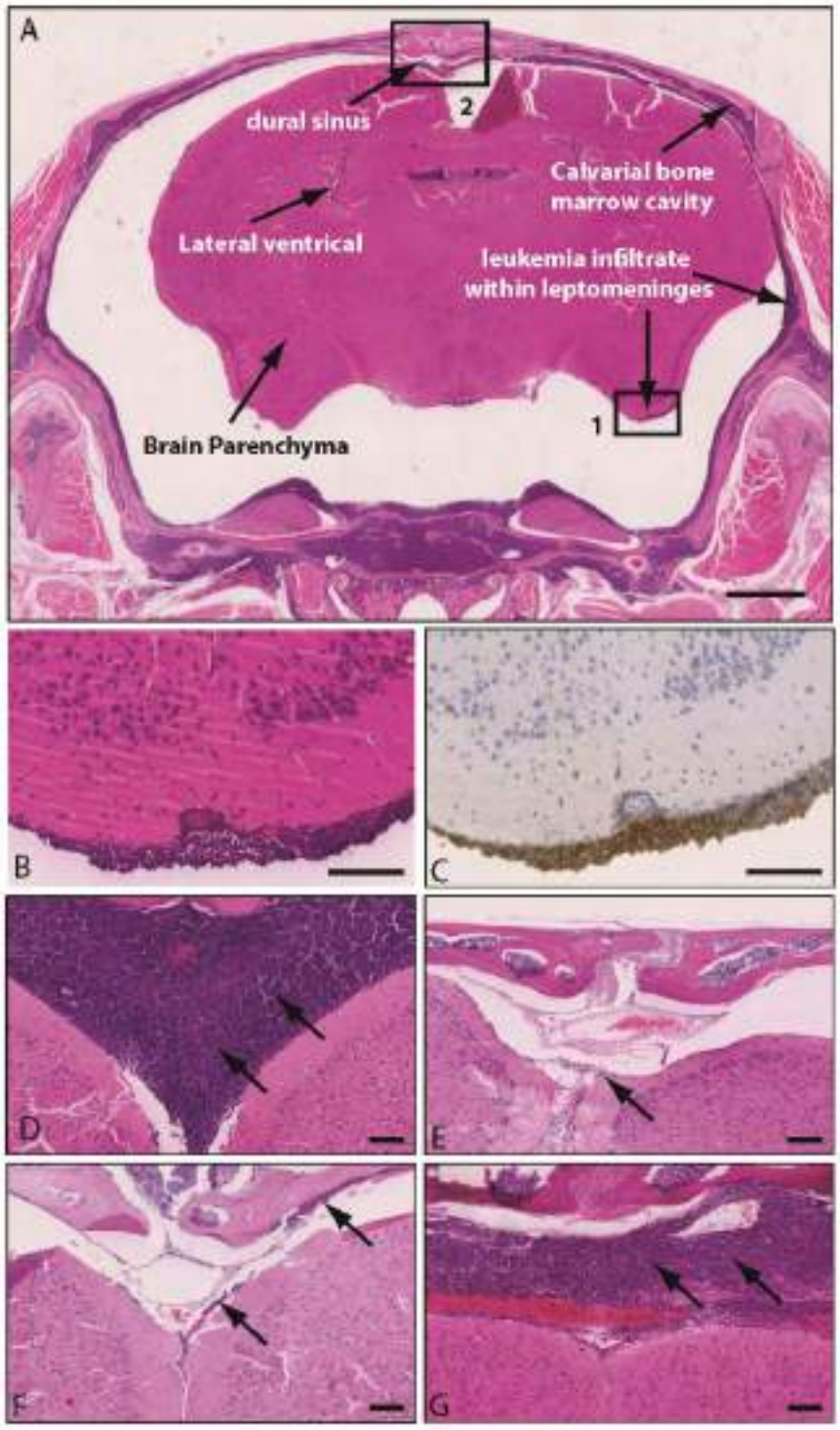

Supplementary Figure 7. SLIEW transduced Xenograft CNS histological sections.

A. H&E stained low powered image of a coronal section through the brain and skull of $1a^{SLIEW}$ with major structures and areas of leukaemia infiltrate marked with arrows. Scale bar is 1 mm. Leukaemic deposit on the surface of the brain in the region marked in box 1 is shown in detail in **B** (stained with H&E) and in **C** (stained with anti-human CD45). Scale bars are 100µm. **D-G** H&E stained detail of the dural sinus region, marked by box 2 in **A**, showing varying degrees of leukaemic infiltrate of the leptomeninges marked by arrows, in xenografts from; $4b^{SLIEW}$ (**D**), $2a^{SLIEW}$ (also representative of $2b^{SLIEW}$) (**E**), $3a^{SLIEW}$ (also representative of $3b^{SLIEW}$) (**F**) and $1a^{SLIEW}$ (also representative of $1b^{SLIEW}$)(**G**). Scale bars are 100µm.

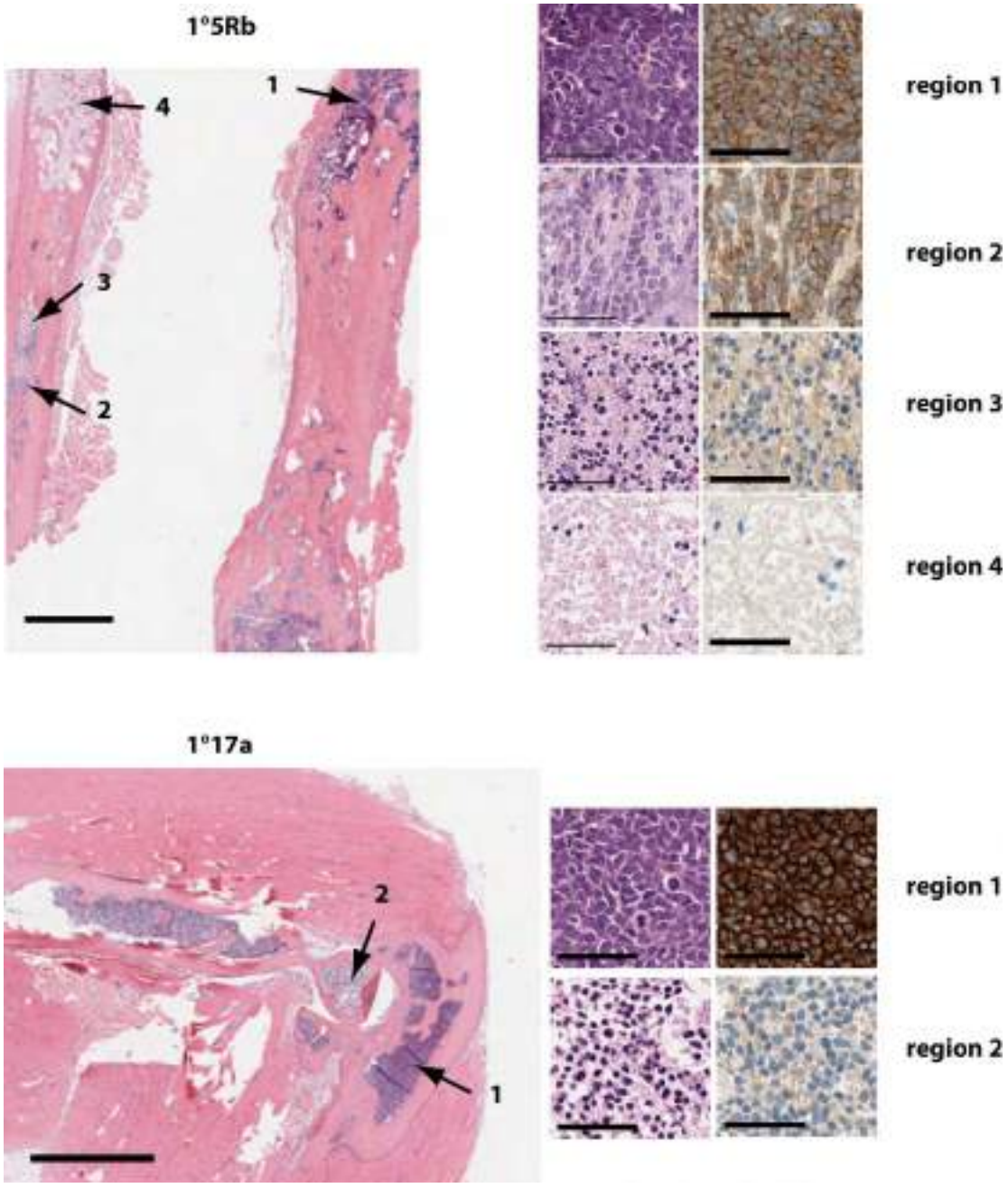

Supplementary figure 8. Histological sections of additional xenografts showing both A and B type morphology. Upper and lower left hand panels show low magnification image of H&E stained sections of fibia and sternum and of the fore limb of xenografts derived from a relapsed iAMP21-ALL (1°5Rb) and a high hyperdiploid ALL respectively (1°17a). Right hand panels show high magnification H&E and human anti-CD19 stained images of regions marked in the left hand panels by arrows. Regions 1 and 2 of the 1°5Rb section and region 1 of the 1°17a section show A-type morphology. Region 3 and 4 of 1°5Rb and region 2 of 1°17a show B type morphology. Scale bars are 1500um and 50um for low and high magnification images respectively.

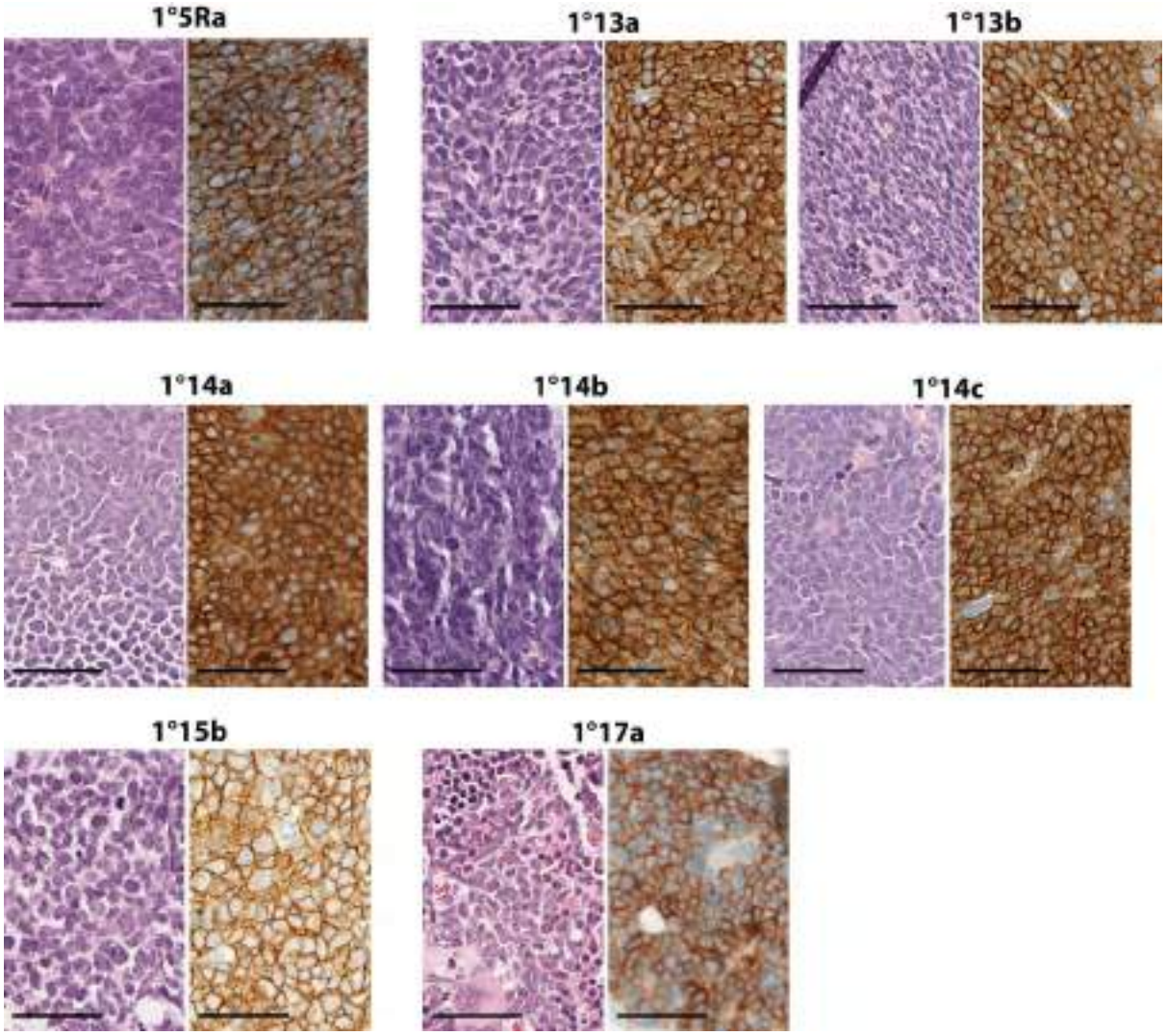

Supplementary Figure 9. Histological sections of additional xenografts showing A type morphology only. High magnification images of bone marrow sections stained with H&E and CD19 taken from tibias, fibias or sternum of additional primografts. The regions shown are representative of all bone marrow observed in a single section of 1 or 2 bones. Scale bars are 50µm.

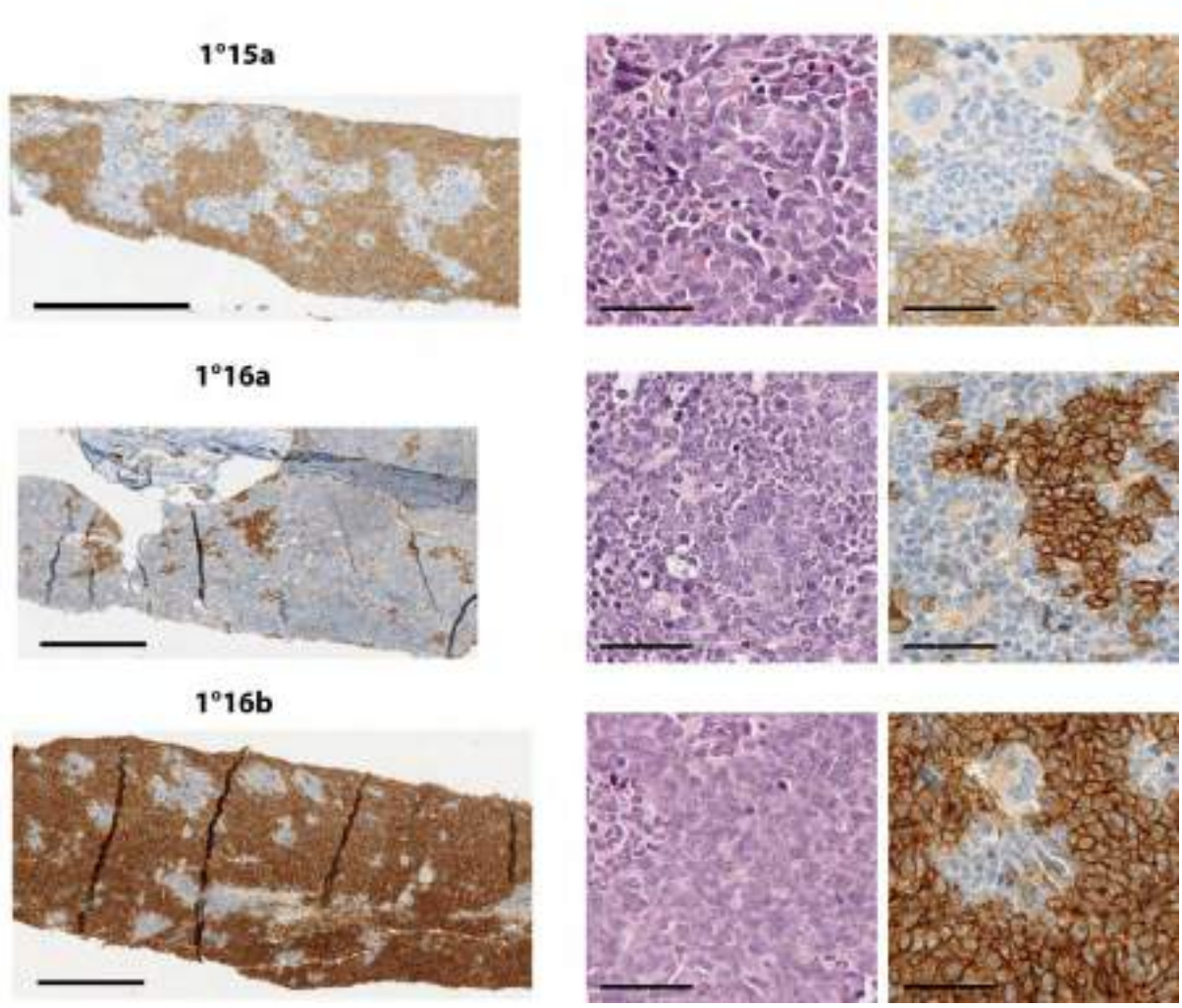

Supplementary Figure 10. Histological sections of additional xenografts showing patches of A-type morphology infiltrating apparently normal mouse bone marrow. Left hand panels show low magnification images of human anti-CD19 stained sections of iAMP21 xenografts showing areas of positively and negatively stained cells. Right hand panels show high magnification H&E and anti-CD19 staining for the same sections. In all three sections infiltrating leukaemia cells are organized into clumps with non-infiltrated areas resembling normal mouse bone marrow. The images shown are representative of a single section of 1 or 2 bones. Scale bars 300 and 50um for low and high magnification images respectively.

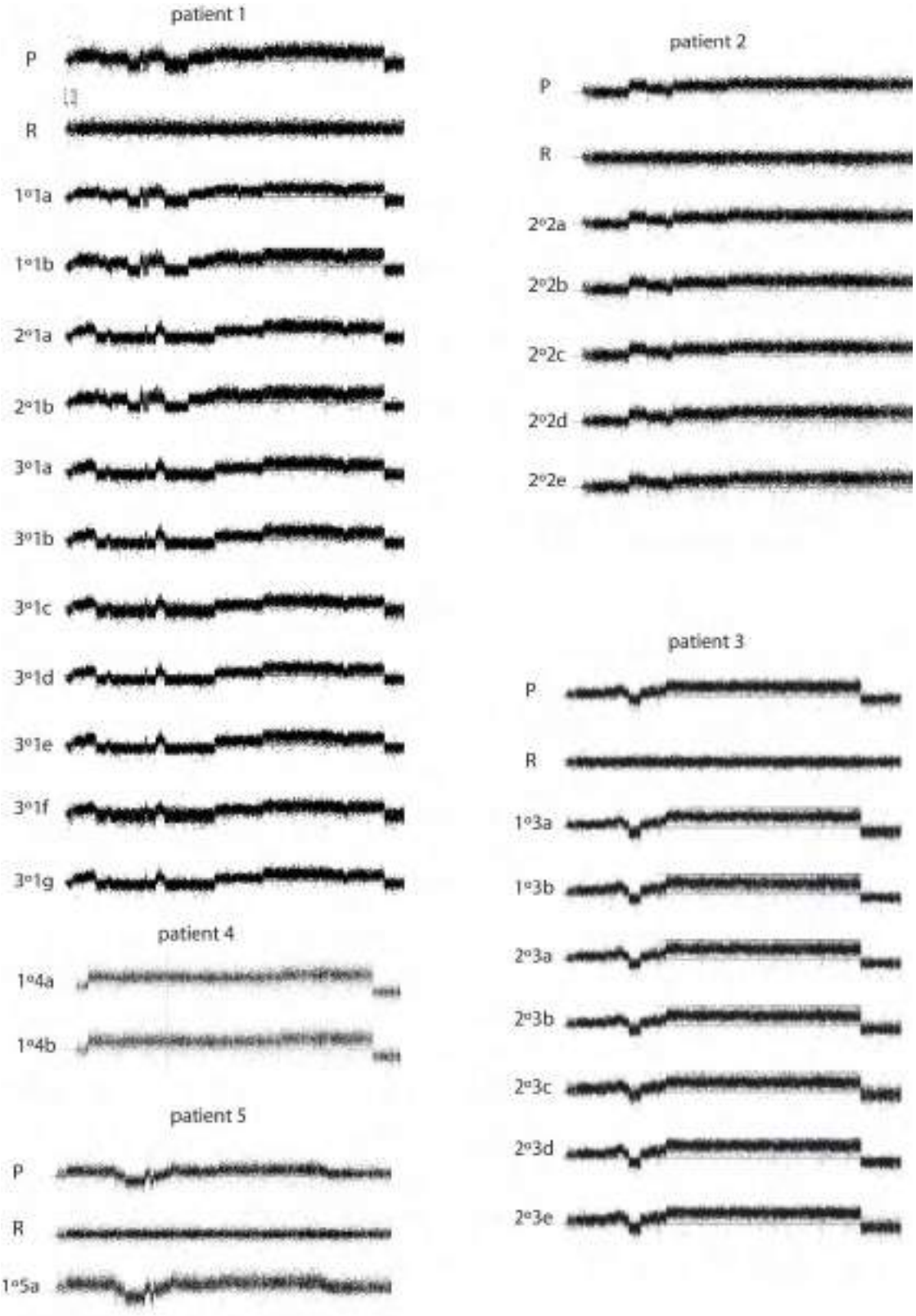

Supplementary Figure 11. SNP6.0 chromosome 21 CN profiles for all patient and xenograft samples analysed.

Samples from presentation (P), remission (R) and xenografts. With the exception of patient 1, profiles were indistinguishable between patient leukemia and/or across xenograft samples.

Supplementary Tables

Supplementary Table 1. Karyotypes and demographic details of iAMP21-ALL patient samples used to create xenografts

Patient registration number	ID this study	Presentation (P) /relapse (R)	Karyotype*	Age (years)	Sex	Previously published patient ID	
						A	B
23229	1	P	47,XX,+10,der(21)r(21)(q?)[10]	10	F	437	1
19578	2	P	48,XY,+X,?t(6;20)(p1;q1),?t(7;9)(p1;p2), i(9)(q10),+12,der(21)(q?)[9]	11	M	426	
21567	3	P	52,XX,+9,-12,-12,+7mar[cp4]	8	F	430	14
23317	4	R	45,X,del(X)(q22),del(1)(p13),der(9;17)(q10; q10),del(10)(q22),del(11)(q14), add(21)(q22)[4]/46,idem,+mar[4]	17	F	439	
24259	5	P	46,XX,t(2;16)(p1?2;q2?3),-21,+mar[5]	13	F	447	7
Samples which failed to engraft							
19578**	2	R	Karyotype not available no RUNX1 amplification	11	M	426	45
9028	6	P	46,X,add(X)(q26-q28),?7, der(21)dup(21)(q?)[8]	10	F	511	28
9864	7	P	47,XY,dup(21)(q?),+dup(21)(q?)[6]	10	M	512	18

Age and white blood cell count (WBC) are at diagnosis. *Normal population excluded from abnormal karyotypes. ** Sample was from a case which relapsed in the CNS with no evidence for iAMP21 by interphase FISH of the bone marrow indicating that the blast count was low in this sample. Previously published IDs refer to previous publications; **A** - Harrison *et al* 2014(12) **B** - Ryan *et al* 2016(3).

Supplementary Table 2. Karyotypes and demographic details of iAMP21-ALL with bone marrow trephines used for histological comparison with iAMP21-ALL derived xenografts.

Patient registration number	ID this study	Presentation (P) /relapse (R)	Karyotype**	Age (years)	Sex	Previously published patient ID	
						A	B
23229*	1	P	47,XX,+10,der(21)r(21)(q?)[10]	10	F	437	1
24259*	5	P	46,XX,t(2;16)(p1?2;q2?3),-21,+mar[5]	13	F	447	7
5754	8	P	46,XY,ider(21)(q10)dup(21)(q?)[6]	9	M	478	
21795†	9	P	46,XX[20]	8	F		
23982	10	P	46,XX,add(21)(q2?2)[6]	8	F	444	21
25821	11	P	46,XX,del(7)(q22),del(8)(q22),add(15)(q26), der(21)[cp10]	25	F		
27421†	12	P	N/A	14	F		

Age was at diagnosis. *Patients 1 and 5 were also used to create xenografts. †iAMP21 identified by interphase FISH. **Normal population excluded from abnormal karyotypes. N/A, not available. Previously published IDs refer to previous publications; **A** - Harrison *et al* 2014(12) **B** - Ryan *et al* 2016(3).

Supplementary Table 3. **Karyotypes and demographic details of additional B-ALL patient samples used to create xenografts examined histologically.**

Patient registration number	ID this study	Genetic subtype /Presentation (P) or relapse (R)	Karyotype**	Age (years)	Sex	Previously published patient ID	
						A	B
22322	12	iAMP21/P	46~47,XX,+?X,add(7)(p22),del(11)(q23), del(13)(q12q14),dup(21)(q22),+r	8	F	433	15
20724*	13	iAMP21/P	46,XY	3	M	429	16
23299	14	iAMP21/P	46,XY,der(1)t(1;13)(q2?5;q12),?del(9)(p 2?1),-11,-13,-15,del(16)(q10),-17,-21,+3mar[5]/45,XY, rob(15;21)(q10;q10)?c[5]	10	M	439	43
22340	15	iAMP21/P	46,XX,ider(21)?inv dup(21)(q1q2)[9]	10	F	434	11
24259*	5	iAMP21/R	N/A	13		447	7
10420†	16	ETV6-RUNX1/P	46,XY,del(6)(q13q23),add(8p),der(12) ?t(12;22)(p?;q?),+21,-22,der(22)t(?;22)	3	M		
2058	17	Hyperdiploid/P	52,XX,+X,+9,add(9)(p13),+14,+18,+21, +21	4	F		

Age was at diagnosis. *iAMP21 identified by interphase FISH. † *ETV6-RUNX1* fusion identified by FISH. ** Normal population excluded from abnormal karyotypes. N/A, not available. Previously published IDs refer to previous publications; **A** - Harrison *et al* 2014(12) **B** - Ryan *et al* 2016(3).

Supplementary Table 4. Details of xenograft generation and ex-vivo analysis of tumour load.

Xenograft id /sex of host	time to cull (weeks)	spleen weight/tumour load**	CD19	CD10	+ve cells Bone marrow	+ve cells Spleen
Patient 1; CD19 92%, CD10 94%, CD34 93%.						
primary mice; $1.6x10^6$ cells transplanted / mouse						
1°1a/M	38	1.13g/NA	+ve	+ve	40%	36%
1°1b/M	30	1.43g/NA	+ve	+ve	60%	23%
secondary mice; $2x10^4$ 1°1B bone marrow cells transplant / mouse						
2°1a/F	35	$0.8g/6x10^8$	+ve	+ve	50%	32%
2°1b/F	24	0.33g/NA	+ve	+ve	42%	33%
tertiary mice; $2x10^6$ 2°1A spleen cells transplanted / mouse						
3°1a/F	22	$1.77g/8.9x10^8$	+ve	+ve	Ficol 90%	Ficol 95%
3°1b/F	23	$1.6g/1.4x10^9$	+ve	+ve	Ficol 98%	Ficol 95%
3°1c/M	28	enlarged*/$3.7x10^8$	+ve	+ve	NA	Ficol 96%
3°1d/M	28	enlarged*/$1.8x10^8$	+ve	+ve	NA	Ficol 94%
3°1e/M	27	$1.6g/8x10^8$	+ve	+ve	92%	Ficol 95%
3°1f/M	27	$1.78g/1.5x10^9$	+ve	+ve	NA	Ficol 96%
3°1g/M	12	$0.66g/2.5x10^9$	+ve	+ve	71%	Ficol 99%
Patient 2; CD19 85%, CD10 83%, CD34 80%						
primary mouse $3.3x10^5$ transplanted						
1°2a/NA	29	0.285g/NA	+ve	+ve	40%	27%
secondary mice; $1x10^6$ 1°2A spleen cells transplanted / mouse						
2°2a/F	8	0.34g/NA	+ve	+ve	6%	5%
2°2b/F	22	$0.73g/2.4x10^8$	+ve	+ve	18%	Ficol 85%
2°2c/F	22	$1.3g/1x10^9$	+ve	+ve	NA	NA
2°2d/F	29	$1.0g/1.4x10^9$	+ve	+ve	NA	Ficol 97%
2°2e/F	29	$1.5g/6x10^8$	+ve	+ve	NA	NA
2°2f/F	23	$1.2g/1.5x10^9$	+ve	+ve	51%	Ficol 80%
2°2g/M	25	$1.3g/2.5x10^8$	+ve	+ve	48%	Ficol 85%
Patient 3; CD19 85%, CD10, 84%, CD34 83%						
primary mice; $1x10^6$ cells transplanted / mouse						
1°3a/F	25	enlarged*/NA	+ve	+ve	21%	Ficol 87%
1°3b/F	35	$3.6g/4x10^9$	+ve	+ve	NA	Ficol 99%
Secondary mice; $1x10^6$ 1°3B spleen cells transplanted / mouse.						
2°3a/M	16	$2.53g/4x10^9$	+ve	+ve	38%	Ficol 92%
2°3b/M	16	$0.28g/3.6x10^6$	+ve	+ve	29%	Ficol 97%
2°3c/M	15	$2.4g/7x10^8$	+ve	+ve	36%	Ficol 95%
2°3d/M	16	$3.6g/3.22x10^9$	+ve	+ve	34%	Ficol 95%
2°3e/M	16	$1.3g/6x10^8$	+ve	+ve	32%	Ficol 95%
Patient 4; NA						
Primary mice; $2x10^5$ cells transplanted / mouse.						
1°4a/F	22	enlarged*/NA	+ve	+ve	NA	Ficol 95%
1°4b/F	20	$1.3g/1.4x10^9$	+ve	+ve	NA	Ficol 97%
1°4c/F	20	$1.3g/9.7x10^8$	+ve	+ve	95%	Ficol 96%

Patient 5; CD19 56%, CD10 59%, CD34 62%.						
Primary mouse; $1x10^6$ cells transplanted.						
1°5a/F	53	$0.80g/6x10^8$	+ve	+ve	NA	Ficol 80%
Transduced with pSLIEW and analysed by in-vivo imaging and histology post-mortem						
Patient 1; $1.5x10^6$ transduced 3°1E spleen cells transplanted / mouse						
$1a^{SLIEW}$ /F	16	0.53g/NA	+ve	NA	NA	Ficol 92%
$1b^{SLIEW}$ /F	18	0.88g/NA	+ve	NA	NA	Ficol 92%
Patient 2; $1.5x10^6$ transduced 2°2E spleen cells transplanted / mouse						
$2a^{SLIEW}$ /F	16	0.40g/NA	+ve	NA	NA	Ficol 86%
$2b^{SLIEW}$ /F	14	$0.55g/2x10^8$	+ve	NA	NA	Ficol 89%
Patient 3; $1.5x10^6$ transduced 2°3D spleen cells transplanted / mouse						
$3a^{SLIEW}$ /F	15	0.23g/NA	+ve	NA	NA	Ficol 85%
$3b^{SLIEW}$ /F	15	0.27g/NA	+ve	NA	NA	Ficol 94%
Patient 4; $1.5x10^6$ transduced 1°4B spleen cells transplanted / mouse						
$4a^{SLIEW}$ /F	15	0.83g/NA	+ve	NA	NA	Ficol 89%
$4b^{SLIEW}$ /F	14	0.81g/NA	+ve	NA	NA	Ficol 79%

Ficol indicates that the sample was purified by Ficol gradient separation. * Spleen weight not recorded but splenomegaly noted. ** Tumour load refers to the total number of cells isolated (a variable proportion of cells are lost in the course of purification over Ficol). NA data not available.

Supplementary table 5. Xenograft Immunophenotypic data.

id	%CD19+ve (MFI)		%CD10+ve (MFI)		%CD34+ve (MFI)		%CD38+ve (MFI)	
	BM	spleen	BM	spleen	BM	spleen	BM	spleen
Patient 1; CD19 92%, CD10 94%, CD34 93%.								
primary mice								
1°1a	**100** (10920)	**100** (11171)	**100** (21462)	**100** (18458)	**52** (5224)	**51** (4623)	**18** (567)	**10** (474)
1°1b	**100** (10133)	**100** (12845)	**99** (9642)	**100** (53563)	**44** (2940)	**78** (12640)	**3** (340)	**50** (1579)
secondary mice								
2°1a	**100** (28751)	**100**	**100** (61831)	**100**	**100** (19668)		**97** (4334)	
2°1b	**100** (21717)	**100** (24860)	**100** (59035)	**100** (80485)	**96** (17696)	**97** (20089)	**88** (3028)	**91** (3234)
tertiary mice								
3°1a	**100**	**100** (21614)	**100**	**100** (51772)		**90** (14720)		**93** (4281)
3°1b	**100**	**100** (16847)	**100**	**100** (42753)		**70** (11325)		**72** (3170)
3°1c		**100** (18589)		**100** (43906)		**82** (11666)		**82** (3113)
3°1d		**100** (16382)		**100** (46420)		**72** (12212)		**75** (3170)
3°1e	**100**	**100** (17125)	**100**	**100** (45972)		**69** (11586)		**73** (3132)
3°1f		**100** (19948)		**100** (48138)		**77** (12268)		**83** (3095)
3°1g	**100** (24742)	**100** (15819)	**100** (68666)	**100** (46872)	**94** (17696)	**89** (12815)	**97** (4831)	**94** (3847)
Patient 2; CD19 85%, CD10 83%, CD34 80%								
primary mouse								
1°2a	**100**	**100**	**100**	**100**				
secondary mice								
2°2a	**100** (14349)	**100 (**12815**)**	**100** (51397)	**100 (**38352**)**	**82** (15065)	**84** (12296)	**85** (3089)	**63** (1881)
2°2b	**100**	**100** (10341)	**100**	**100** (38723)		**89** (11020)		**39** (1204)
2°2c		**100**		**100**				
2°2d		**100** (8262)		**100** (36547)		**88** (10341)		**16** (762)
2°2e	**100** (9664)	**100** (7629)	**100** (45750)	**100** (30305)	**91** (14283)	**89** (9513)	**29** (1125)	**1** (700)
2°2f	**100** (11171)	**100** (12101)	**100** (61831)	**100** (54881)	**93** (17490)	**92** (14652)	**55** (1902)	**51** (1652)
2°2g	**100**	**100**	**100**	**100**				
Patient 3; CD19 85%, CD10, 84%, CD34 83%								
primary mice								
1°3a	**100**	**100**	**100**	**100**				
1°3b		**100**		**100**				
Secondary mice								
2°3a	**100** (21110)	**100** (26956)	**100**(143642)	**100**(124849)	**84** (29236)	**81** (26384)	**19** (1784)	**6** (1320)
2°3b	**100**	**100** (22448)	**100**	**100**(130499)		**56** (25038)		**1** (1188)
2°3c	**100**	**100** (20137)	**100**	**100**(127329)		**82** (27739)		**3** (1290)
2°3d	**100**	**100** (24161)	**100**	**100**(130499)		**78** (25038)		**3** (1188)
2°3e	**100**	**100** (19807)	**100**	**100**(120329)		**66** (24334)		**1** (1127)
Patient 4;								
Primary mice								
1°4a		**100** (17367)		**100** (30743**)**		**60** (7817)		**19** (807)
1°4b		**100** (17820)		**100** (54747)		**80** (18853)		**66** (2428)
1°4c	**100**	**100** (18941)	**100**	**100** (37984)		**35** (8027)		**88** (3532)

Patient 5; CD19 56%, CD10 59%, CD34 62%.								
Primary mouse								
1°5a	**100**	**100**	**100**	**100**				
Transduced with pSLIEW and analysed by in-vivo imaging and histology post-mortem								
Patient 1								
1a^{SLIEW}		**100**		**100**				
1b^{SLIEW}		**100** (16926)		**100** (57616)		**71** (13235)		**86** (3400)
Patient 2								
2a^{SLIEW}		**100**		**100**				
2b^{SLIEW}		**100**		**100**				
Patient 3								
3a^{SLIEW}		**100** (18720)		**100**(145780)		**48** (27345)		**0** (1744)
3b^{SLIEW}		**100**		**100**				
Patient 4								
4a^{SLIEW}		**100** (15709)		**100** (36635)		**58** (9156)		**77** (3046)
4b^{SLIEW}		**100**		**100**				

Mean fluorescence intensity (MFI). Gray boxes indicate that no sample was available for analysis.

Supplementary table 6. Bone marrow histology of additional xenografts.

Xenograft ID	Genetic sub-type	Sample	Morphology type*
1°5Ra	iAMP21	femur/sternum	A
1°5Rb	iAMP21	femur/sternum	A/B
1°13a	iAMP21	tibia	A
1°13b	iAMP21	tibia/sternum	A
1°14a	iAMP21	tibia/sternum	A
1°14b	iAMP21	tibia/sternum	A
1°14c	iAMP21	tibia	A
1°15a	iAMP21	tibia/sternum	WT/A
1°15b	iAMP21	tibia/sternum	A
1°16a	iAMP21	humerus/sternum	WT/A
1°16b	iAMP21	humerus/sternum	WT/A
2°17a	ETV6-RUNX1	tibia	A
1°18a	Hyperdiploid	forelimb/sternum	A/B

*WT (wild type morphology similar to control NSG mice), A and B (as defined in the main text and shown in figures 2, and Supplementary figures 3 and 7).

Supplementary Table 7. Copy number abnormalities (CNA) identified by SNP6.0 array analysis in patients and xenografts.

Y; clonal CNA present

N; CNA not detected

S; sub-clonal CNA present

Patient 1 concordant CNA

				1°		2°		3° Xenografts							
Chr	**abnormality**	**genomic position**	**patient**	**a**	**b**	**a**	**b**	**a**	**b**	**c**	**d**	**e**	**f**	**g**	**genes**
4	del (CN 1)	153060000-153272000	Y	Y	Y	Y	Y	Y	Y	Y	Y	Y	Y	Y	FBXW7
6	del (CN 1)	25950000-26285000	Y	Y	Y	Y	Y	Y	Y	Y	Y	Y	Y	Y	33 genes TRIM38, HIST1H1A- HIST1H2B1
6	del (CN 0)	26135000-26255000	Y	Y	Y	Y	Y	Y	Y	Y	Y	Y	Y	Y	18 genes HIST1H1E- HIST1H2B1
7	del (CN 1)	49850000-51565000	Y	Y	Y	Y	Y	Y	Y	Y	Y	Y	Y	Y	VWC2, ZPBP, C7orf72, IKZF1, FIGNL1, DDC, GRB10, COBL
7	del (CN 1)	65800000-66475000	Y	Y	Y	Y	Y	Y	Y	Y	Y	Y	Y	Y	9 gene TPST1-TYW1
7	del (CN 1)	137889000-138447000	Y	Y	Y	Y	Y	Y	Y	Y	Y	Y	Y	Y	TRIM24, SVOPL, ATP6VOA4
7	del (CN 1)	138489000-141624000	Y	Y	Y	Y	Y	Y	Y	Y	Y	Y	Y	Y	30 genes KIAA1549- OR9A4,
7	del (CN 1)	142060000-142202000	Y	Y	Y	Y	Y	Y	Y	Y	Y	Y	Y	Y	none
7	del (CN 1)	154559000-155465000	Y	Y	Y	Y	Y	Y	Y	Y	Y	Y	Y	Y	9 genes DPP6-RBM33
8	del (CN 1)	60030000-60446000	Y	Y	Y	Y	Y	Y	Y	Y	Y	Y	Y	Y	TOX
12	del (CN 1)	11825000-12025000	Y	Y	Y	Y	Y	Y	Y	Y	Y	Y	Y	Y	ETV6 (exons 1-5), RNU6-19 (Exons1&2)
12	del (CN 1)	121160000-121274000	Y	Y	Y	Y	Y	Y	Y	Y	Y	Y	Y	Y	UNC119B, MIR4700, ACADS, SPPL3
13	del (CN 1)	48984700-49074000	Y	Y	Y	Y	Y	Y	Y	Y	Y	Y	Y	Y	RB1 (ex ?17-end), LPAR6, RCBTB2 (ex 1-3)
15	del(CN 1)	93158000-94982000	Y	Y	Y	Y	Y	Y	Y	Y	Y	Y	Y	Y	FAM174B, ASB9P1, LOC100507217, CHD2, RGMA, MCTP2

Patient 1 discordant CNA

3	del (CN 1)	32375000-32552000	N	N	N	Y	N	Y	Y	Y	Y	Y	Y	Y	CMTM 8, 7, 6
9	del (CN 1)	19540000-32310000	N	N	N	Y	N	Y	Y	Y	Y	Y	Y	Y	40 genes SLC24A2- MOB3B,
9	del (CN 0)	19620000-27194000	N	N	N	Y	N	Y	Y	Y	Y	Y	Y	Y	37 genes SLC24A2, MLLT3-TEK
10	trisomy		Y	N	N	N	N	N	N	N	N	N	N	N	

Patient 2 concordant CNA

				2° xenografts						
Chr	**Abnormality**	**genome position**	**patient**	**a**	**b**	**c**	**d**	**e**	**f**	**genes**
3	del (CN 1)	35528000-35684000	Y	Y	Y	Y	Y	Y	Y	ARPP21 (exons1&2)
6	del (CN 1)	46699000-47018000	Y	Y	Y	Y	Y	Y	Y	PLA2G7, LOC100287718, MEP1A, GPR116, GPR110
7	del (CN 1)	50150000-51210000	Y	Y	Y	Y	Y	Y	Y	C7orf72, IKZF1, FIGNL1, DDC, GRB10, COBL
7	del (CN 1)	109732000-158646480	Y	Y	Y	Y	Y	Y	Y	many
8	del (CN 1)	53567000-53596000	Y	Y	Y	Y	Y	Y	Y	RB1CC1 (exons 9-20)
9	del (CN 1)	0-39500000	Y	Y	Y	Y	Y	Y	Y	many
9	del (CN 0)	20365000-22404000	Y	Y	Y	Y	Y	Y	Y	32 genes MLLT3-CDKN2B-AS1
9	amp (CN 3)	70950000-141067840	Y	Y	Y	Y	Y	Y	Y	many
11	del (CN 1)	63950000-64000000	Y	Y	Y	Y	Y	Y	Y	STIP1, FERMT3, TRPT1, NUDT22, DNAJC4, VEGFB
12	del (CN 1)	11846000-11930000	Y	Y	Y	Y	Y	Y	Y	ETV6 (ex 2)
13	amp (CN 3)	67315000-115150780	Y	Y	Y	Y	Y	Y	Y	many
16	del (CN 1)	3781000-3824000	Y	Y	Y	Y	Y	Y	Y	CREBBP (ex 1-19)
20	del (CN 1)	56168000-56690000	Y	Y	Y	Y	Y	Y	Y	ZBP1, PMEPA1, MIR4532
22	del (CN 1)	22320000-22540000	Y	Y	Y	Y	Y	Y	Y	TOP3B
X	WCG		Y	Y	Y	Y	Y	Y	Y	

Patient 2 discordant CNA

2	del (CN 1)	74000000-86000000	N	N	N	S	N	N	N	Many TPRKB-ST3GAL5
12	trisomy		Y	N	N	N	N	N	N	
X	iso(p)		N	N	N	S	Y	N	N	many
X	del (CN 1)	47248000-47342000	N	N	Y	S	S	S	S	ZNF157, ZNF41

Patient 3 concordant CNA

				1°		2° xenografts					
Chr	**Abnormality**	**genomic position**	**patient**	**a**	**b**	**a**	**b**	**c**	**d**	**e**	**genes**
4	amp (CN 3)	70125000-70238000	Y	Y	Y	Y	Y	Y	Y	Y	UGT2B28
5	trisomy		Y	Y	Y	Y	Y	Y	Y	Y	
10	trisomy		Y	Y	Y	Y	Y	Y	Y	Y	
12	del (CN 1)	104860000-105042000	Y	Y	Y	Y	Y	Y	Y	Y	CHST11 (ex 2&3)
14	trisomy		Y	Y	Y	Y	Y	Y	Y	Y	
17	trisomy		Y	Y	Y	Y	Y	Y	Y	Y	
17	del (CN 1)	62590000-62665000	Y	Y	Y	Y	Y	Y	Y	Y	SMURF2 (ex 15-18)
X	del (CN 1)	1380000-1604000	Y	Y	Y	Y	Y	Y	Y	Y	CSF2RA, IL3RA, SLC25A6, ASMTL-AS1, ASMTL, P2RY8(UTR).

Patient 3 discordant CNA

9	trisomy		Y	Y	N	N	N	N	N	N	
12	del (CN 1)	0-24500000	S	S	N	N	N	N	N	N	
12	del (CN 1)	11950000-32460000	N	N	S	N	N	N	N	N	ETV6 (ex 3-7) many genes BICD1 (exon 1-4)
X	trisomy		Y	S	Y	Y	S	Y	S	S	

patient 4 concordant CNA

			1° xenografts		
Chr	**Abnormality**	**genomic position**	**1**	**2**	**genes in region**
1	complex	89800000-121500000	Y	Y	many
1	del (CN 0)	152550000-152590000	Y	Y	LCE3, LCE3B, LCE3A
1	del (CN 1)	196720000-196800000	Y	Y	CFHR3, CFHR1
2	del (CN 1)	184500000-184600000	Y	Y	ZNF804A
5	del (CN 1)	142674000-142750000	Y	y	NR3C1
5	del (CN 0)	142674000-142724350	Y	y	NR3C1
9	del (CN 1)	0-34150000	Y	y	many including CDKN1A/B
9	del (CN 0)	21954000-22119000	y	y	CDKN1A, CDKN1B, CDKN1B-AS1
9	del (CN 1)	37000000-37350000	Y	Y	PAX5, ZCCHC7
10	del (CN 0)	98350000-98700000	Y	Y	PIK3AP1, LCOR
11	del (CN1)	82000000-134963460	Y	Y	many
12	del (CN 1)	11800000-12000000	Y	Y	ETV6 intragenic
12	del (CN 0)	111760000-112060000	Y	Y	CUX2, FAM109A, SH2B3, ATXN2
12	del (CN 1)	133350000-133800000	Y	Y	COLGA3, CHFR, ZNF605, ZNF26, ZNF84, ZNF140, ZNF10, ZNF268, ANHX
13	del (CN 1)	44600000-45050000	Y	Y	SERP2
20	del (CN 1)	1500000-1630000	Y	Y	SIRPD, SIRPB1, SIRPG

Patient 4 discordant CNA

4	del (CN 1)	174060000-174260000	Y	N	GALNT7, HMGB2
4	amp (CN2)	69350000-69500000	N	Y	UGT2B17
10	del (CN 1)	90000000-135534000	Y	Y	many
10	del (CN 1))	80800000-126400000	N	N	many
10	del (CN 0)	98015000-98060000	N	Y	BLNK
14	amp (CN 3)	36900000-43900000	Y	N	13 genes SLC25A21- LRFN5
14	del (CN 1)	43900000-107349520	Y	N	many
16	del (CN 1)	3770000-3920000	Y	N	CREBBP
17	amp (CN 1)	25300000-27450000	N	N	many
17	amp (CN 2)	25920000-26300000	Y	Y	many
17	amp (CN 1)	25300000-25920000	Y	Y	many
22	del (CN 1)	37630000-37740000	N	N	RAC2, CYTH4

Patient 5 concordant CNA

			patient		1° xenograft	
Chr	**Abnormality**	**genomic position**	**presentation**	**relapse**	**a**	**genes**
2	del (CN 1)	63776000-75095000	y	Y	Y	many
4	del (CN 1)	71760000-71900000	y	Y	Y	MOB1B, DCK
6	del (CN 1)	26126000-26260000	y	Y	Y	16 genes HIST1H1E- HIST1H2BH

Patient 5 discordant CNA

1	del (CN 1)	234612000-235540000	N	N	S	8 genes TARBP1- ARID4B,
2	del (CN 1)	2322000-8874000	S	N	Y	LOC100506274, LOC339788, LINC00299, ID2, KIDINS220 (ex 1)
3	del (CN 1)	114080000-114680000	S	N	Y	ZBTB20
3	del (CN 1)	45900000-48250000	S	Y	N	37 genes CCR9-CAMP
5	del (CN 1)	158088000-158149000	N	N	S	EBF1 exons 1-5
5	del (CN 1)	158380000-158580000	N	Y	N	EBF1 exons 10-16
12	CN-LOH	53500000-133721800	Y	Y	N	many
12	del (CN 1)	111050000-112135000	S	N	Y	12 genes TCTN1- ACAD10

Supplementary Table 8. Regions of chromosome 21 copy number change that occurred in xenografts from patient 1.

start	end	size	CN change
0	16446092	16446092	0
16446092	17302313	856221	1
17381183	17697572	316389	-2
17697723	18163458	465735	-1
18163544	18174691	11147	0
18177172	20521089	2343917	-1
20521648	21760268	1238620	0
21760283	22125481	365198	-2
22125690	22517120	391430	0
22517189	23343710	826521	-2
23345771	26533474	3187703	0
26533786	28305871	1772085	-1
28306308	29236061	929753	-2
29243377	31443709	2200332	-1
31447334	31680485	233151	0
31683535	33949423	2265888	-1
33949543	48096945	14147402	0

Supplementary Table 9. MLPA values for patients and their xenografts. A score of 1 indicates normal copy number. Examples with clear evidence for CN changes between samples are highlighted (loss by shades of red and gain by shades of green).

	Patient 1		
	patient	xenografts	
Target		2°1b	3°1g
01a_EBF1_ex16	1.035	0.855	1.142
01b_EBF1_ex14	1.086	1.114	0.952
01c_EBF1_ex10	1	0.974	1.16
01d_EBF1_ex1	0.965	0.958	1.127
02a_IKZF1_ex1	0.588	0.499	0.596
02b_IKZF1_ex2	0.649	0.481	0.56
02c_IKZF1_ex3	0.616	0.451	0.598
02d_IKZF1_ex4	0.583	0.454	0.603
02e_IKZF1_ex5	0.639	0.435	0.567
02f_IKZF1_ex6	0.609	0.566	0.529
02g_IKZF1_ex7	0.636	0.511	0.597
02h_IKZF1_ex8	0.55	0.49	0.622
03a_JAK2_ex23		0.844	0.825
03b_CDKN2A_ex5	0.936	0.987	0
03c_CDKN2A_ex2a	1.022	0.897	0
03d_CDKN2B_ex2	1.021	0.919	0
04a_PAX5_ex10	1.032	0.97	1.255
04b_PAX5_ex8	0.942	0.828	1.236
04c_PAX5_ex7		0.966	0.994
04d_PAX5_ex6	1.015	0.974	1.183
04e_PAX5_ex5	0.981	1.086	0.996
04f_PAX5_ex2	1.149	0.795	1.171
04g_PAX5_ex1	0.981	0.938	1.149
05a_ETV6_ex1A	0.97	1.048	0.969
05b_ETV6_ex1B	1.003	1.1	0.948
05c_ETV6_ex2	0.201	0	0.527
05d_ETV6_ex3	0.401	0.511	0.473
05e_ETV6_ex5	0.616	9	0.627
05f_ETV6_ex8	0.986	0.945	1.122
06a_BTG1-AREA1	0.972	0.913	1.043
06b_BTG1_AREA2	0.893	0.919	1.106
06c_BTG1_ex2	1.038	0.967	1.14
06d_BTG1_ex1	1.06	0.815	1.262
07a_RB1_ex6	0.955	0.874	1.137
07b_RB1_ex14	1.015	94	0.967
07c_RB1_ex19	0.117	0	0
07d_RB1_ex24	0.118	0	0
07e_RB1_ex26	0.095	0	0
08a_SHOX_area	1.01	0.918	0.995
08b_CRLF2_ex4	0.997	0.942	1.09
08c_CSF2RA_ex10	1.043	0.993	0.924
08d_IL3RA_ex1	0.98	1.038	0.852
08e_P2RY8_ex2	0.987	0.943	1.106
08f_ZFY_ex4	0	-1	-1

Patient 2						
	patient	secondary xenografts				
Target		2°2c	2°2d	2°2b	2°2e	2°2f
01a_EBF1_ex16	0.975	0.965	0.918	0.945	1.054	1.019
01b_EBF1_ex14	0.948	0.949	1.025	0.953	0.84	0.901
01c_EBF1_ex10	0.965	0.994	1.06	1.061	1.083	1.083
01d_EBF1_ex1	0.898	1.051	1.067	0.998	1.157	1.078
02a_IKZF1_ex1	0.485	0.541	0.602	0.579	0.538	0.551
02b_IKZF1_ex2	0.539	0.53	0.583	0.536	0.572	0.543
02c_IKZF1_ex3	0.547	0.535	0.541	0.555	0.579	0.579
02d_IKZF1_ex4	0.55	0.539	0.599	0.59	0.598	0.622
02e_IKZF1_ex5	0.544	0.534	0.544	0.526	0.574	0.559
02f_IKZF1_ex6	0.575	0.494	0.497	0.494	0.447	0.53
02g_IKZF1_ex7	0.483	0.599	0.665	0.598	0.61	0.588
02h_IKZF1_ex8	0.509	0.611	0.648	0.602	0.645	0.635
03a_JAK2_ex23	0.565	0.426	0.432	0.409	0.368	0.396
03b_CDKN2A_ex5	0	0	0	0	0	0
03c_CDKN2A_ex2a	0	0	0	0	0	0
03d_CDKN2B_ex2	0	0	0	0	0	0
04a_PAX5_ex10	0.512	0.591	0.622	0.587	0.669	0.625
04b_PAX5_ex8	0.5	0.732	0.823	0.862	0.703	0.637
04c_PAX5_ex7	0.552	0.659	0.72	0.677	0.497	0.482
04d_PAX5_ex6	0.512	0.592	0.662	0.633	0.629	0.653
04e_PAX5_ex5	0.56	0.545	0.593	0.54	0.451	0.491
04f_PAX5_ex2	0.508	0.548	0.616	0.647	0.605	0.591
04g_PAX5_ex1	0.516	0.556	0.595	0.639	0.624	0.632
05a_ETV6_ex1A	1.344	1.016	1.047	1.027	0.942	0.919
05b_ETV6_ex1B	1.307	0.939	0.948	0.97	0.875	0.891
05c_ETV6_ex2	0.596	0.522	0.532	0.506	0.456	0.476
05d_ETV6_ex3	1.378	0.915	0.921	0.89	0.856	0.924
05e_ETV6_ex5	1.39	1.069	1.047	1.076	1.146	1.123
05f_ETV6_ex8	1.283	1.07	1.074	1.068	1.126	1.101
06a_BTG1-AREA1	1.215	0.945	0.973	0.924	0.997	0.95
06b_BTG1_AREA2	1.247	1.02	1.039	1.021	1.043	1.04
06c_BTG1_ex2	1.258	1.078	1.093	1.033	1.138	1.104
06d_BTG1_ex1	1.141	1.229	1.391	1.395	1.256	1.307
07a_RB1_ex6	0.909	1.013	1.06	0.991	1.087	1.077
07b_RB1_ex14	0.984	0.962	0.998	0.939	0.894	0.924
07c_RB1_ex19	0.93	1.031	1.094	1.012	0.919	0.926
07d_RB1_ex24	1.004	1.048	1.023	1.029	0.85	0.955
07e_RB1_ex26	0.998	0.954	0.876	0.88	0.83	0.877
08a_SHOX_area	1.404	1.315	1.26	1.332	1.651	1.347
08b_CRLF2_ex4	1.446	1.34	1.486	1.343	1.46	1.536
08c_CSF2RA_ex10	1.496	1.268	1.205	1.111	1.351	1.221
08d_IL3RA_ex1	1.353	1.384	1.506	1.433	1.328	1.232
08e_P2RY8_ex2	1.252	1.52	1.717	1.657	1.893	1.637
08f_ZFY_ex4	1000	1000	1000	1000	1000	1000

Patient 3							
	Patient	xenografts					
Target		1°3b	2°3c	2°3a	2°3e	2°3b	2°3d
01a_EBF1_ex16	1.356	1.432	1.506	1.529	1.449	1.553	1.507
01b_EBF1_ex14	1.306	1.403	1.319	1.298	1.323	1.319	1.423
01c_EBF1_ex10	1.405	1.223	1.571	1.596	1.522	1.621	1.512
01d_EBF1_ex1	1.363	1.511	1.521	1.621	1.574	1.56	1.429
02a_IKZF1_ex1	1.01	1.047	1.051	1.059	1.041	1.038	0.987
02b_IKZF1_ex2	0.964	0.969	1.022	1.083	1.051	1.037	0.999
02c_IKZF1_ex3	0.978	1.042	1.053	1.09	1.096	1.089	1.063
02d_IKZF1_ex4	0.949	1.033	1.034	1.17	1.098	1.14	1.066
02e_IKZF1_ex5	1	0.95	1.019	1.063	1.054	1.048	0.994
02f_IKZF1_ex6	1.109	0.901	0.891	0.915	0.916	0.994	1.018
02g_IKZF1_ex7	0.941	1.198	1.143	1.164	1.168	1.102	1.077
02h_IKZF1_ex8	1.037	1.183	1.153	1.239	1.213	1.185	1.094
03a_JAK2_ex23		0.722	0.652	0.676	0.719	0.783	0.836
03b_CDKN2A_ex5	1.227	1.011	1.054	1.154	1.116	1.104	1.009
03c_CDKN2A_ex2a	1.348	1.171	1.018	1.037	1.033	1.022	0.964
03d_CDKN2B_ex2	1.215	1.128	1.076	1.142	1.116	1.074	1.034
04a_PAX5_ex10	1.096	1.275	1.214	1.239	1.185	1.164	1.121
04b_PAX5_ex8	1.334	1.676	1.42	1.156	1.213	1.138	1.242
04c_PAX5_ex7		1.391	1.084	0.848	0.919	0.909	1.095
04d_PAX5_ex6	1.231	0.938	0.983	1.189	1.162	1.19	1.113
04e_PAX5_ex5	1.309	0.798	0.729	0.913	0.97	0.923	0.973
04f_PAX5_ex2	1.213	1.063	1.008	1.106	1.105	1.158	1.05
04g_PAX5_ex1	1.207	1.06	1.089	1.145	1.077	1.136	1.046
05a_ETV6_ex1A	0.838	1.009	0.912	0.85	0.915	0.91	0.939
05b_ETV6_ex1B	0.843	0.926	0.882	0.826	0.855	0.877	0.875
05c_ETV6_ex2	0.856	1.001	0.942	0.868	0.883	0.909	0.944
05d_ETV6_ex3	0.868	0.541	0.737	0.758	0.791	0.792	0.864
05e_ETV6_ex5	0.86	0.709	1.106	1.017	1.083	1.02	1.04
05f_ETV6_ex8	0.85	0.68	1.028	0.964	1.008	1.007	0.974
06a_BTG1-AREA1	1.003	0.933	0.941	0.95	0.948	0.977	0.922
06b_BTG1_AREA2	1.136	1.031	0.989	1.013	0.988	1.064	0.976
06c_BTG1_ex2	0.91	1.085	1.098	1.081	1.065	1.132	1.045
06d_BTG1_ex1	0.953	1.322	1.114	1.295	1.231	1.304	1.086
07a_RB1_ex6	1.079	1.013	1.026	1.093	0.992	1.049	0.985
07b_RB1_ex14	0.998	0.938	0.871	0.817	0.841	0.863	0.917
07c_RB1_ex19	0.875	1.016	0.929	0.914	0.911	0.922	0.962
07d_RB1_ex24	0.926	0.987	0.918	0.953	0.91	0.954	0.978
07e_RB1_ex26	0.933	0.885	0.855	0.884	0.835	0.913	0.958
08a_SHOX_area	1.305	1.204	1.202	1.374	1.186	1.18	1.279
08b_CRLF2_ex4	1.325	1.191	1.445	1.454	1.209	1.239	1.437
08c_CSF2RA_ex10	0.579	0.451	0.35	0.379	0.216	0.195	0.408
08d_IL3RA_ex1	0.583	0.412	0.301	0.377	0.24	0.199	0.402
08e_P2RY8_ex2		0.562	0.453	0.514	0.282	0.237	0.441
08f_ZFY_ex4		-1	-1	-1	-1	-1	-1

Patient 5		
Target	patient	primary xenograft 1°5a
01a_EBF1_ex16	0.777	0.536
01b_EBF1_ex14	0.771	0.554
01c_EBF1_ex10	0.928	1.006
01d_EBF1_ex1	0.865	0.988
02a_IKZF1_ex1	0.97	1.025
02b_IKZF1_ex2	1.005	1.004
02c_IKZF1_ex3	0.956	1.003
02d_IKZF1_ex4	0.966	1.028
02e_IKZF1_ex5	1	1.011
02f_IKZF1_ex6	1.09	0.994
02g_IKZF1_ex7	0.905	0.975
02h_IKZF1_ex8	0.964	1.013
03a_JAK2_ex23		0.976
03b_CDKN2A_ex5	0.998	0.564
03c_CDKN2A_ex2a	1.004	0.542
03d_CDKN2B_ex2	1.017	0.979
04a_PAX5_ex10	0.904	1.032
04b_PAX5_ex8	0.971	0.93
04c_PAX5_ex7	1.143	0.948
04d_PAX5_ex6	0.98	1.05
04e_PAX5_ex5	1.013	1.018
04f_PAX5_ex2	1	1.062
04g_PAX5_ex1	0.988	1.042
05a_ETV6_ex1A	1.025	0.995
05b_ETV6_ex1B	1	1.002
05c_ETV6_ex2	1.019	1.014
05d_ETV6_ex3	1	1.035
05e_ETV6_ex5	1	1.033
05f_ETV6_ex8	0.991	1.02
06a_BTG1-AREA1	1.022	0.986
06b_BTG1_AREA2	1.031	0.938
06c_BTG1_ex2	0.983	1.001
06d_BTG1_ex1	1.011	0.995
07a_RB1_ex6	1.022	1.022
07b_RB1_ex14	1.039	1.031
07c_RB1_ex19	1.01	0.906
07d_RB1_ex24	1.2	0.949
07e_RB1_ex26	0.982	0.914
08a_SHOX_area	0.984	1.019
08b_CRLF2_ex4	1.038	1.041
08c_CSF2RA_ex10	1.008	1.018
08d_IL3RA_ex1	1	1.031
08e_P2RY8_ex2	0.979	1.04
08f_ZFY_ex4	0	-1

References for supplementary methods.

1. Bomken S, Buechler L, Rehe K, et al. Lentiviral marking of patient-derived acute lymphoblastic leukaemic cells allows in vivo tracking of disease progression. Leukemia. 2013;27(3):718-721.
2. Williams MT, Yousafzai YM, Elder A, et al. The ability to cross the blood-cerebrospinal fluid barrier is a generic property of acute lymphoblastic leukemia blasts. Blood. 2016;127(16):1998-2006.
3. Ryan SL, Matheson E, Grossmann V, et al. The role of the RAS pathway in iAMP21-ALL. Leukemia. 2016; 30:1824-1831.
4. Conway T, Wazny J, Bromage A, et al. Xenome--a tool for classifying reads from xenograft samples. Bioinformatics. 2012;28(12):i172-178.
5. Li H, Durbin R. Fast and accurate short read alignment with Burrows-Wheeler transform. Bioinformatics. 2009;25(14):1754-1760.
6. Li H, Durbin R. Fast and accurate long-read alignment with Burrows-Wheeler transform. Bioinformatics. 2010;26(5):589-595.
7. Cibulskis K, Lawrence MS, Carter SL, et al. Sensitive detection of somatic point mutations in impure and heterogeneous cancer samples. Nat Biotechnol. 2013;31(3):213-219.
8. DePristo MA, Banks E, Poplin R, et al. A framework for variation discovery and genotyping using next-generation DNA sequencing data. Nat Genet. 2011;43(5):491-498.
9. Van der Auwera GA, Carneiro MO, Levy-Moonshine A, et al. From FastQ data to high confidence variant calls: the Genome Analysis Toolkit best practices pipeline. Curr Protoc Bioinformatics. 2013;43:11.10. 1-33.
10. McLaren W, Pritchard B, Rios D, Chen Y, Flicek P, Cunningham F. Deriving the consequences of genomic variants with the Ensembl API and SNP Effect Predictor. Bioinformatics. 2010;26(16):2069-70.
11. Robinson JT, Thorvaldsdottir H, Winckler W, et al. Integrative genomics viewer. Nat Biotechnol. 2011;29(1):24-6.
12. Harrison CJ, Moorman AV, Schwab C, et al. An international study of intrachromosomal amplification of chromosome 21 (iAMP21): cytogenetic characterization and outcome. Leukemia. 2014;28(5): 1015-1021.